ITER PHYSICS BASIS

CHAPTER 5

PHYSICS OF ENERGETIC IONS

TABLE OF CONTENTS

ITER PHYSICS BASIS

CHAPTER 5: PHYSICS OF ENERGETIC IONS'

ITER Physics Expert Group on Energetic Particles, Heating and Current Drive*
ITER Physics Basis Editors**

ABSTRACT. Physics knowledge (theory and experiment) in energetic particles relevant to design of a reactor-scale tokamak is reviewed and projections for ITER are provided in this Chapter of the ITER Physics Basis. The review includes single particle effects such as classical alpha-particle heating and toroidal field ripple loss as well as collective instabilities that might be generated in ITER plasmas by energetic alpha-particles. The overall conclusion is that fusion alpha-particles are expected to provide an efficient plasma heating for ignition and sustained burn in the next step device. The major concern are localized heat loads on the plasma facing components produced by alpha-particle loss which might affect their life time in a tokamak-reactor.

LIST OF AUTHORS for CHAPTER 5 [in alphabetical order after chair, co-chair]

* ITER Physics Expert Group on *Energetic Particles, Heating and Current Drive*: J. Jacquinot (chair), S. Putvinski (co-chair), G. Bosia, A. Fukuyama, R. Hemsworth, S. Konovalov, Y. Nagashima, W. M. Nevins, F. Perkins, K. Rasumova, F. Romanelli, K. Tobita, K. Ushigusa, J. W. Van Dam, V. Vdovin, S. Zweben
Additional contributing authors: H. L. Berk, D. Borba, B. N. Breizman, R. Budny, J. Candy, C. Z. Cheng, A. Fasoli, G. Y. Fu, W. Heidbrink, R. Nazikian, G. Martin, F. Porcelli, M. Redi, M. N. Rosenbluth, G. Sadler, S. E. Sharapov, D. A. Spong, R. White, F. Zonca

** ITER Physics Basis Editors: F. W. Perkins, D. E. Post, N. A. Uckan, M. Azumi, D. J. Campbell, N. Ivanov, N. R. Sauthoff, M. Wakatani
Additional contributing editors: W. M. Nevins, M. Shimada, J. Van Dam

5.1. INTRODUCTION

Self-sustained ignition of an ITER thermonuclear plasma depends on heating by highly energetic alpha particles (i.e., ^{4}He ions) produced from fusion reactions. The alpha particles, born at 3.5 MeV in a reacting deuterium-tritium plasma (envisioned for use in ITER), transfer their energy mostly to thermal electrons, which in turn heat the plasma ions through collisions. Accumulation of the slowed-down, low energy alpha particles as "helium ash" needs to be prevented, since it dilutes the fusion fuel. Another concern is poor confinement of the energetic alpha particles (or other energetic ions in ITER used for current drive or auxiliary heating), caused either by single-particle "ripple" loss or by anomalous transport due to collective instabilities. Such losses can not only reduce the alpha particle heating efficiency, but also lead to excessive heat loading and damage to plasma-facing components (e.g., first walls and divertor plate structure). Some of these problems have been studied in existing experiments and analyzed theoretically. Reviews have been previously given of the detailed behavior of alpha particles [5.1-5.3] and of various energetic particle issues specific to ITER operation [5.4, 5.5] In this chapter, we summarize, and apply to ITER, current knowledge about major issues that have been identified: alpha particle production and heating (Section 5.2), single-particle confinement (Section 5.3), collective instabilities and anomalous transport (Section 5.4), and possible alpha particle control methods (Section 5.5). Alpha-particle diagnostics which are planned for the experimental study of ignition and ash control in ITER are discussed in Chapter 7.

Before beginning that summary, we briefly describe how ITER differs from present experimental devices with respect to energetic ion physics. Many years of tokamak research have shown that the fast ions used to heat tokamaks normally do so with high efficiency and without causing problems. These high energy ions are either externally introduced by neutral beam injection or internally generated by minority ion cyclotron wave resonant heating. Sometimes, however, the fast ion heating efficiency has been reduced due to non-axisymmetries such as toroidal field ripple, or due to energetic-ion-driven collective instabilities such as various Alfvén

eigenmodes. To help assess whether such problems will occur for alpha particle heating in ITER, Table 5-I compares the fast ion (subscript *f*) physics parameters of current experiments with the anticipated alpha particle parameters of ITER.

The first thing to note from Table 5-I is that the alpha particle heating power density in ITER will actually be lower than the fast ion heating power density in present large tokamaks. The reason is that, in ITER, the plasma energy density will be only slightly larger, whereas the plasma energy loss rate should be much lower, than in present experiments. Thus the relative density and the beta value for the alpha particles in ITER will be smaller than those for the neutral beam and wave-heated fast ions currently used to heat large tokamaks. On the other hand, the alpha particle beta value in ITER will be a few times larger than those obtained in the JET and TFTR deuterium-tritium experiments cited in Table 5-I.

Next to be noted from Table 5-I is that the orbit size δ/a for alpha particles in ITER will be comparable to that for fast ions in present beam-heated experiments. Hence the single-particle confinement of alphas in ITER should be very good, except possibly for toroidal field ripple loss.

Table 5-I also shows that the dimensionless fast ion pressure gradient $R\nabla\beta_f$, which drives collective fast ion instabilities, will be smaller for alpha particles in ITER than for beam-heated fast ions in present experiments. However, the ratio of the alpha particle velocity to the Alfvén speed, $v_f / v_A(0)$, will exceed unity in ITER – which is typically the parameter range in which fast ion-driven Alfvén instabilities have been seen in existing experiments.

An important parameter not shown in Table 5-I is the plasma pulse length, which is 1000 seconds for ITER but only a few seconds for present experiments. The long pulse length requires that the first-wall components be carefully protected and actively cooled to prevent the formation of localized hot spots, which could cause uncontrolled impurity influx or damage to the wall. Therefore even a few-percent loss of alpha particles to an unprotected location on the ITER first wall could be a problem, whereas a similar fast ion loss fraction over the time scale of a few seconds has not been a problem for present experiments.

Another difference of a self-heated ignition experiment like ITER with auxiliary heated tokamaks has to do with the fact that, in contrast to fast ions produced by neutral beam or RF waves applied from outside, there is little external control of the alpha particles. Some control schemes have been proposed.

As it was mentioned above, there are two major design issues associated with energetic-particle loss in ITER: 1) reduction in the plasma heating and 2) local heat loads on the plasma facing components. These issues have clearly a direct impact on the choice of major plasma parameters of the ignited plasma and on the design of the plasma facing components. It was found that the alpha-particle heat loads are much more restrictive in ITER than the loss of plasma heating. Indeed, if the energy confinement time in ITER has a degradation with the total heating power, $\tau_E \propto P^{-\alpha}$, then from the plasma power balance point of view the alpha-particle loss will be equivalent to a degradation in the energy confinement time by factor $(1-L)^{1-\alpha}$, where L is alpha-particle power loss fraction. For example, ITERH-93P scaling, with $\alpha = 0.67$, predicts ~10% of ignition margin for ITER (see Chapter 2) and, therefore, ignition is possible if alpha-particle loss <30% . At the same time, very small grazing angles of the lost particles make distribution of the losses over the first wall very uneven and very sensitive to the details of the wall shape. The peaking factors can be as high as 200-300, and loss of more than 5% alpha-particles could be damaging for the first wall in ITER.

In the case of energetic ions produced by NB or ICRH, the total heating power is six times less than the alpha-particle heating in ITER and both limitations are more or less equal - heat loads on the wall are becoming an issue when there is a noticeable degradation in the total heating power due to the loss.

5.2. CLASSICAL PHYSICS OF ENERGETIC PARTICLE CONFINEMENT AND PLASMA HEATING

Based on the experimental results on the energetic particle heating in the present tokamaks, it is expected that the fusion alpha-particles in ITER type plasmas will be well confined to heat plasma efficiently and their slowing down and energy transfer to the main plasma will be defined by classical Coulomb collisions with the background electrons and ions. Therefore, we shall start this review with a description of a classical theory of alpha-particle heating in tokamaks.

5.2.1. Classical Interaction with the Main Plasma

Based on earlier works of Spitzer [5.6] and Sivukhin [5.7], Stix [5.8] derived the following formula for the slowing-down rate of beam ions in a plasma:

$$\frac{dE}{dt} = -\frac{2E}{\tau_s}\left[1+\left(\frac{E_{crit}}{E}\right)\right]^{3/2} \qquad (5\text{-}1)$$

where E is alpha-particle energy, τ_s is the characteristic Spitzer slowing down time on field electrons, and E_{crit} is the so-called critical energy. These are given by:

$$\tau_s = \frac{3\sqrt{2\pi}T_e^{3/2}}{\sqrt{m_e}m_b A_D}\ , \quad A_D = \frac{ne^4\ln\Lambda}{2\pi\varepsilon_0^2 m_b^2}$$

$$E_{crit} = \left(\frac{3\sqrt{\pi}}{4}\right)^{2/3}\left(\frac{m_i}{m_e}\right)^{1/3}\frac{m_b}{m_i}T_e$$

for a pure hydrogen plasma (ion mass m_i)

$$E_{crit} = 14.8\frac{A_b}{A_i^{2/3}}T_e$$

For high energies of the beam ions the energy loss is mainly due to collisions with plasma electrons. The collisions with ions become more important when the beam ions are slowed down. At $E = E_{crit}$ the energy loss on ions and electron is equal. Below this energy ion collisions are dominant. The total energy transfer to plasma ions and electrons are equal for an injection energy of $E = 2.41\ E_{crit}$ [5.9]. For a higher injection energy, electrons are heated predominantly and vice versa.

Evident electron heating by alpha particles or by energetic particles has been confirmed in several tokamaks. In particular, TFTR [5.10] and JET [5.11] deuterium-tritium experiments observed alpha heating that is consistent with theory. Moreover, abundant experiments on the deceleration of energetic particles also indicate that alpha heating in ITER will obey classical theory if the alpha particles are well confined in the plasma. Figure 5-2 shows the measured slowing-down time compared with the theoretical prediction over the range $0.5 \leq E_b/E_{crit} \leq 35$, extending from where electron friction is dominant to where bulk ion friction is dominant. The slowing-down time of energetic ions agrees well with classical theory over a wide range of fast ion energies, plasma temperatures, and densities, as supported by experiments using NB ions and charged fusion products [5.3, 5.12, 5.13]. In TFTR deuterium-tritium experiments, pellet charge exchange measurements [5.14] confirmed that the slowing-down energy spectra of alpha particles in an MHD-quiescent plasma matched the prediction from a Fokker-Planck post-TRANSP processor code, which had classical modeling with stochastic ripple diffusion [5.15]. The classical plasma heating by fusion alpha-particles was observed in DT experiments at JET [5.11].

5.2.2. Alpha Particle Density and Beta Profiles

Most alpha particles in ITER will be produced by thermal deuterium-tritium reactions and, as a result, their birth profile will be broad compared with that in TFTR and JET, where tritium was injected as a beam into a deuterium plasma. Based on classical slowing-down physics, the local values of n_α/n_e and β_α/β, where n_α and β_α are the fast alpha particle density and beta values,

with $\beta = \beta_e + \beta_i + \beta_\alpha$ the total plasma beta value, are approximately determined as functions only of the temperature, independent of the electron density n_e [5.16]. If we assume that the ion and electron temperatures are about the same ($T_i = T_e = T$) and take $Z_{eff} = 1.5$ with carbon impurities, then n_α/n_e and β_α/β increase as the temperature goes up, as shown in Fig. 5-1. For a representative ITER temperature of $\langle T \rangle = 10.5$ keV, we have $n_\alpha/n_e \approx 0.1\%$ and $\beta_\alpha/\beta \approx 5\%$. In the core region where temperatures are expected to exceed 20 keV, the values of n_α/n_e and β_α/β can be as high as ~0.8% and ~15%, respectively.

5.2.3. Neoclassical Diffusion of Alpha Particles

In present tokamaks, some fusion-product charged particles can experience first-orbit loss because of the relatively low plasma current I_p and small minor radius a. In TFTR deuterium-tritium experiments, the alpha particle loss decreased as the plasma current increased, and this was well explained with a first-orbit loss model [5.17]. In ITER, with high current and sufficiently large minor radius, the first-orbit loss will be negligibly small (0.1% for a broad alpha particle birth profile just after a sawtooth crash).

The transport of alpha particles in the core region is believed to obey conventional neoclassical diffusion under the assumption of toroidal symmetry. In the outer region, however, broken toroidal symmetry caused by “ripple” due to the discrete number of toroidal field coils can give rise to rapid diffusion or convection (described in Section 5.3). Experimentally, fast ions are well confined in the core region, with small diffusion coefficient D_{fast}, consistent with theory. The pitch angle dependence of 1 MeV tritons and 3 MeV protons escaping to a detector located at the bottom of TFTR indicated a negligible diffusion coefficient [5.18]. In TFTR deuterium-tritium experiments, D_{fast} for alpha particles was 0.01–0.1 m^2/s as determined by three separate measurements [5.12, 5.19]. In JET, the experimental results for triton burnup match a classical diffusive model with $D_{fast} = 0.1$ m^2/s [5.20]. A similar result has been reported for JT-60U, indicating $D_{fast} = 0.05$ m^2/s when toroidal field ripple is small (~0.3% at the plasma surface)

[5.21]. Also, there is much experimental evidence showing that the diffusion coefficient for neutral beam-injected ions is ~0.1 m^2/s or less [5.3].

Thus, one of the remarkable results on fast ion transport is that their diffusion coefficient is small, on the order of 0.1 m^2/s, which is comparable to the neoclassical level and ten times smaller than the typical value for anomalous thermal ion transport observed in tokamaks. This result may be evidence that energetic ions are not subject to the mechanism responsible for the bulk of heat loss. The smallness of the measured fast ion diffusion coefficient may be explained by "orbit averaging" of small-scale plasma turbulence over the large orbits of the fast ions [5.22, 5.23]; this transport reduction mechanism could, however, be less effective in larger tokamaks if the turbulence size scale increases with machine size [5.24].

When pitch angle scattering on background ions becomes comparable to electron drag, the alpha particles diffuse radially while slowing down. Their corresponding neoclassical diffusion coefficient in a toroidally symmetric system is [5.25]

$$D^{\alpha}_{scatt} \cong 0.24\,\varepsilon^{1/2}\,\frac{v_{\alpha}^{\,2}}{\tau_s\,\Omega_{p\alpha}^{\,2}} \qquad (5\text{-}2)$$

where v_α is the alpha particle birth energy, $\varepsilon = r/R$ the inverse aspect ratio, τ_s the slowing-down time, and $\Omega_{p\alpha} = Z_\alpha e B_p / m_\alpha c$ is the poloidal gyrofrequency, calculated with the poloidal magnetic field B_p. For ITER parameters, D^{α}_{scatt} is approximately 0.01–0.1 m^2/s. For a 12 MA post-sawtooth-crash profile, the alpha particle loss arising from this neoclassical diffusion is estimated to be 0.2%, much smaller than the ripple loss.

On the basis of neoclassical transport, a bootstrap current from the fast alpha particles is expected. The results from a model calculation that used the ACCOME code [5.26] are shown in Fig. 5-3. In the calculation, temperature and density profiles for a 21 MA ignited plasma at 1.5 GW fusion power are assumed; 50 MW neutral beams with an energy of 1 MeV are injected co-tangentially; and other key parameters are $Z_{eff} = 1.5$ and $q(0) = 1$. Since the bootstrap current

from the alpha particles (0.44 MA) is much smaller than that from the bulk plasma electrons and ions (4.44 MA), it has little impact on the MHD equilibrium. However, for a low-current (12 MA) advanced steady-state scenario in which the bootstrap current is expected to comprise 80% of the total current, the bootstrap current of the alpha particles will not be negligible and it could contribute to the MHD equilibrium.

5.3. TOROIDAL FIELD RIPPLE LOSS AND OTHER SINGLE-PARTICLE EFFECTS

5.3.1. Mechanisms and Loss Channels of Toroidal Field Ripple Loss

Potentially significant loss of alpha particles can occur in ITER-size machines due to toroidal field (TF) ripple, i.e., toroidally asymmetric perturbations of the toroidal magnetic field due to the discreteness of the TF coils. The TF ripple amplitude is defined as

$$\delta = \frac{B_{\max} - B_{\min}}{B_{\max} + B_{\min}},$$

where $B_{\max}$ and $B_{\min}$ are the magnitudes of the toroidal magnetic field calculated at two points having the same radial and vertical coordinates in the meridian cross section but different toroidal coordinates — one under a TF coil, and another midway between two neighboring coils. The TF magnetic system in ITER has 20 coils, with a maximum ripple amplitude at the plasma edge of 0.6%. The ripple profile for the ITER plasma cross section, as shown in Fig. 5-4, is typical for tokamaks with moderate aspect ratio (A = 2.5–3.5) and a large number (N > 16) of TF coils. Due to the poloidal variation of the magnetic field on a magnetic surface, the magnetic ripple wells exist only near the equatorial plane and mostly at the outer part of the plasma cross section where the ripple is relatively large.

The effect of TF ripple on the confinement of energetic particles in tokamaks has been well studied both theoretically [5.27–5.29] and experimentally [5.30-5.37]. Efficient numerical codes

have been developed [5.26–5.30, 5.38–5.40] and also validated by comparison with experimental results. This is an area in the physics of the fusion plasmas where models based on first principles are able to produce quite accurate quantitative results.

There are several channels for energetic particle loss that are important for an ITER-type ripple profile. (1) *Convective loss of ripple trapped particles*: Particles born in the ripple well region with a very small parallel velocity $(v_{||}/v) < \delta^{1/2}$ can be trapped in the magnetic well. These particles experience vertical magnetic drift and will be lost. In ITER, particle scattering due to Coulomb collisions will be too small to prevent convective loss. (2) *Collisionless ripple well trapping of banana particles*: Particles following banana orbits have a very small velocity near the turning points and can be trapped in a well if one of the turning points is located in the ripple well region [5.28]. An energetic particle has a very high probability of becoming trapped, within only a few bounce periods. Ripple-trapped particles will drift along a contour of constant magnetic field strength (i.e., nearly vertically in the *R*–*z* plane) until they leave the region with ripple wells and become collisionlessly detrapped from the TF ripple, or until they exit the plasma and strike the wall. For the ripple well boundary shown in Fig. 5-4, most of these particles will be collisionlessly detrapped from the TF ripple. (3) *Residual drift of banana particles*: When the ripple profile is up-down asymmetric (as in ITER), a banana particle that has at least one banana turning point in the ripple well region experiences a residual radial drift [5.41, 5.42]. When the ripple well depths at the upper and lower turning points are different, the banana orbit is not closed and after each bounce period there is a displacement. The resultant average banana drift, $v_b \approx v_{drift}\sqrt{\delta A}$, is rapid on the collisional time scale. Banana-trapped particles with at least one of their banana turning points in the ripple well region can drift outward in radius while the banana turning point stays on a contour of constant magnetic field strength (i.e., moves nearly vertically), until both banana tips exit the ripple well region, or they exit the plasma and strike the first wall.

In addition to prompt convective loss from the ripple well loss cone, other losses can occur through channels that bring particles from the core region of the plasma to the ripple well loss cone. (1) *Collisional scattering* of transit and banana particles in the loss cone is important for

typical ITER conditions, especially for particles that have partially slowed down to energies of several hundred keV, so that scattering on ions is comparable with the slowing down time. The effect significantly increases the particle ripple loss fraction and contributes significantly to the energy loss fraction. (2) *Stochastic ripple diffusion* [5.29] is a very fast and powerful loss channel if it exists. Even outside the ripple well region, ripple perturbations lead to small vertical periodical displacements of the banana turning points, $\Delta z \approx \rho\delta(qA)^{3/2}(\pi N)^{1/2}$, where ρ is the particle Larmor radius. (Radial displacements are prohibited by conservation of particle energy and magnetic moment.) For large ripple magnitude and large particle energy, the orbits become unstable and stochastic. As a result, energetic particles can experience fast radial diffusion and be lost. However, in the ITER-type ripple profile, the ripple magnitude decreases rapidly away from the ripple well boundary, and the stochastic region is very narrow, comparable in width to Δz. Strictly speaking, in this case there is no stochastic diffusion, but rather a widening of the ripple well loss cone by an amount $\sim\rho(\pi qA/N)^{1/2}$.

The major numerical tools for the analysis of ripple loss in tokamaks are orbit-following Monte Carlo codes. Their drawback is the need for extensive computational run time, which limits the statistics for the lost particles. An approach based on a combination of full orbit-following and mapping techniques allows the calculations to be speeded up significantly.

These codes, validated and tested on experimental data, have been applied to ITER conditions in order to evaluate the ripple loss of energetic ions and the peak heat loads on the plasma-facing components [5.43]. Because of the high peaking factors (typical for the loss of energetic particles), the local heat loads in ITER will be more limiting than the total deterioration of the plasma heating efficiency. The magnitude of the ripple in ITER has been adjusted so that the alpha particle ripple loss is low, less than 0.5% in ignited regimes with high plasma current, and the heat loads acceptable. Low-current configurations with reversed magnetic shear were found to be most susceptible to ripple loss. In such configurations the alpha particle loss fraction can be as high as 1.5%, and the local heat loads are close to the maximum acceptable value of 0.5 MW/m^2. The loss fraction for 1 MeV neutral beam ions is somewhat larger (2-3%), but the total neutral

beam power is six times less than the alpha particle power, and the peak heat loads for both alpha particle and neutral beam ion loss are within the allowed limits.

5.3.2. Experimental Results on Fast Ion Ripple Loss

A comprehensive set of fast ion ripple loss experiments has recently been performed on JT-60U, JET, Tore-Supra, and TFTR for the purpose of code validation.

The JT-60U experiments [5.31-5.33] were devoted to verifying the modeling capabilities of the orbit-following Monte Carlo code OFMC, which has been used to predict ripple loss for ITER. In JT-60U, special attention was paid to measuring hot spots on the first wall due to fast ion ripple loss, for which two ripple loss channels (viz., ripple-trapped and banana drift loss channels) were identified. OFMC code predictions agreed well with both the measured positions and the heat flux of the ripple loss channels on the wall, as illustrated in Fig. 5-5. When a radial electric field was included in the particle orbit calculations, the OFMC predictions were improved and could explain the measured two-dimensional profile of the hot spots in detail. In order to estimate the feasibility of operating ITER with reversed ion ∇B drift, ripple losses were compared for upward and downward ion ∇B drift, in plasmas with an ITER-like up-down asymmetric ripple well. No difference with respect to magnitude of the ripple loss was seen between the two experimental situations, guaranteeing the feasibility of ion ∇B drift reversal for H-mode operation in ITER.

Two TF ripple experiments were performed on JET [5.34, 5.35] in which the TF ripple at the outboard midplane was varied in a controlled manner from 1% to 12%. The behavior of the of ion cyclotron heated high-energy minority tail ions was diagnosed with a neutral particle analyzer and gamma radiation, and also from measurements of the “burn up” of deuterium-deuterium fusion-product 1 MeV tritons into 14 MeV neutrons. No unexpected behavior was observed for fast particles (with energies greater than 100 keV); i.e., the fast ion loss was consistent with Monte Carlo calculations of the expected TF ripple loss [5.36]. What remains unexplained is the effect of

the ripple on toroidal plasma rotation, since the observed braking effect was significantly larger than that predicted by theory [5.27].

The loss of ripple-trapped ion cyclotron heated minority tail ions in the energy range of 100-300 keV has been investigated in Tore-Supra with the use of a set of graphite probes mounted in ports between the TF coils [5.37]. Most of the ions are lost on trajectories originating from the boundary of the TF ripple trapping region, as expected. However, anomalously large bursts of fast ion loss have been observed during monster sawteeth, perhaps due to MHD activity near the $q = 1$ surface. Rugged, energy-resolving graphite calorimeter detectors are under development for these studies, which may also be useful as a diagnostic for alpha ripple loss measurements in ITER.

The effect of TF ripple on deuterium-tritium alpha particles in TFTR was measured with the pellet charge exchange diagnostic and escaping alpha particle scintillator detectors. The radial profile of the confined trapped alphas measured by pellet charge exchange shows an empty region near the outboard plasma edge [5.44], which is consistent with modeling of the expected stochastic TF ripple diffusion boundary. The deuterium-tritium alpha loss was measured just below the outer midplane [5.45], and the loss mechanism was tentatively identified, by the pitch angle of the detected alphas, as stochastic ripple diffusion.

An interesting synergistic effect between TF ripple loss and toroidal Alfvén eigenmodes was seen during ion cyclotron wave hydrogen minority heating in TFTR, where a vacuum leak occurred due to fast ion loss localized between TF coils in the ion ∇B drift direction [5.46]. Apparently fast ions were transported outward by the Alfvén instabilities and subsequently lost through ripple trapping.

Recently in triton burnup measurements on JT-60U, an increase in TF ripple loss associated with high-$q(0)$, reversed shear operation has been observed [5.33]. In TFTR plasmas with reversed shear (but no internal transport barrier), beam-injected fast tritium ions were observed to experience 40% loss at large major radius [5.47]. These results are relevant to ITER advanced operation in a low-current scenario.

5.4. COLLECTIVE ALPHA PARTICLE AND ENERGETIC ION INSTABILITIES

A variety of collective instabilities, ranging in frequency from 10 Hz up to 10^9 Hz, may be driven by alpha particles [5.2]. Results from present-day experiments have shown that two classes of instabilities are especially effective in causing anomalous transport of energetic ions: low-frequency MHD-type instabilities, such as the fishbone, internal kink, and ballooning modes, associated with the resonance between the mode frequency and the toroidal precession frequency of the fast particles; and higher frequency instabilities, such as the shear Alfvén gap modes, associated with the resonance at the fast particle poloidal transit/bounce frequency.

5.4.1. Low-Frequency MHD Modes

5.4.1.1. Introduction to fast ions and MHD modes

An important question is the effect that sawteeth and low-frequency MHD perturbations can have on the confinement of alpha particles and other energetic ions. Of equal importance, however, is the profound effect that energetic ions can have on the stability of low-frequency MHD modes in tokamaks. The main physical mechanism is related to the non-MHD behavior of fast ions with magnetically trapped orbits. The banana orbits of trapped particles precess toroidally at a rate determined by the precessional drift frequency, ω_D, which is proportional to the particle energy. For fast ions with energies in the MeV range, ω_{Df} can become larger than the typical frequency, ω, of a low-frequency MHD perturbation. In this case, the energetic ion banana orbits can complete many toroidal revolutions during the time scale of variation for a low-frequency MHD fluctuation, so that the magnetic flux through the toroidal trajectory of the banana center is adiabatically conserved (third adiabatic invariant). This can prevent the growth of low-frequency MHD modes. A kinetic energy principle can be used to evaluate the modified stability threshold

with conservation of the third adiabatic invariant taken into account. This energy principle [5.48, 5.49] was first applied to the stability of ballooning modes [5.50, 5.51] and later found to be relevant in explaining the enhanced stability of internal kink modes [5.52, 5.53] and the occurrence of long sawtooth-suppressed periods (often referred to as "monster sawteeth" [5.54]) in ion cyclotron wave-heated tokamak discharges, in which minority ions are accelerated to very high energies. Similar stabilization may occur in the presence of the fusion alpha particles [5.55, 5.56].

On the other hand, fast ions with somewhat lower energies can interact resonantly with low-frequency MHD modes, the relevant resonance condition being $\omega_{Df} = \omega$. With ω estimated as the thermal ion diamagnetic frequency, ω_{*i}, the condition $\omega_{Df} = \omega_{*i}$ is satisfied by particles with energy $E_f/T_i \approx 2R/r_p$, where r_p is the thermal ion pressure gradient length. The typical fast ion energy of this regime in present tokamak experiments is in the 100 keV range, which is characteristic of neutral beam injection. Obviously, in this regime, the third adiabatic invariant is no longer a relevant constraint. In fact, the resonant fast ions can destabilize [5.57, 5.58] internal kink modes, and this resonant destabilization is thought to be the physical mechanism for fishbone instability, named after the characteristic experimental trace of the associated magnetic fluctuation bursts [5.59]. Note that the resonant interaction becomes relevant not only when the energy of the fast ions is not large enough to effectively decouple them from the MHD mode, but also when the fast ion density exceeds a critical threshold above which a new continuum Alfvén mode (i.e., strongly continuum-damped in the absence of the fast ions) with a frequency $\omega \sim \omega_{Df}$ is driven unstable [5.58]. In the latter case, the energy transfer rate from the fast ions to the mode exceeds the background continuum damping rate.

Just as for internal kink modes, fast ions can either suppress ballooning modes (as already mentioned) or excite them resonantly, the corresponding instability being known in the literature as kinetic ballooning modes [5.60–5.62]. In addition, energetic ions may enhance the stability of a plasma against interchange modes [5.63] localized in the region where $q < 1$.

5.4.1.2. Interaction of energetic ions with sawtooth oscillations

Radial redistribution of deuterium-tritium alpha particles due to sawteeth has been observed on TFTR with the pellet charge exchange diagnostic [5.14, 5.15] and Alpha-CHERS [5.64], although the loss of alphas during sawtooth crashes appears to be very small. An example of the measured radial redistribution of partially thermalized alphas after a sawtooth crash in TFTR is shown in Fig. 5-6. Observations during large sawteeth with ion cyclotron wave heating on JET have shown bursts of escaping 15 MeV protons [5.65] (from the D-^{3}He reaction), although in the absence of sawteeth the confinement of the fast ^{3}He tail ions in JET appears to be classical [5.66]. Neutral beam ions and deuterium-deuterium tritons both seem to be redistributed by sawteeth in JET [5.67]. Present thinking is that the higher the energy of the particles, the less likely they are to be disturbed by sawteeth, and that different types of sawteeth have different effects on the fast particles. Theoretical explanations of the redistribution of fast particles during a sawtooth crash has been offered [5.68, 5.69].

Synergism between sawteeth and other single-particle alpha effects can cause increased alpha particle transport. For example, a large sawtooth crash in ITER could significantly redistribute alpha particles from the inside to the outside of the inversion radius at $r/a \approx 0.5$, leading to a large (but transient) increase in toroidal field ripple-induced alpha particle heat loss onto the wall. Although a large sawtooth crash may redistribute a significant fraction of the alpha heating power in ITER, it is likely that ignition will be maintained since the time scale for alpha particle re-creation (~1 sec) is shorter than the plasma energy loss rate (~5 s). Simulations of these TF ripple and sawtooth effects for alphas in ITER have been performed with the TRANSP code [5.70]. The largest fast ion losses during toroidal Alfvén eigenmode activity were seen in TFTR to occur at sawtooth events [5.71].

On the other hand, sawtooth oscillations may be suppressed by the energetic ions for several confinement times, the sawtooth-free period being limited by the expansion of the region where $q < 1$, up to the point where the $q = 1$ radius approaches almost half the plasma minor radius [5.52]. These long-duration “monster sawteeth” are characterized by saturation of the temperature

and pressure profiles long before the sawtooth crash occurs, indicating that the internal kink instability threshold is reached as a consequence of the evolution of the current density. In JET, sawtooth-free periods of between one to five seconds have been obtained in discharges with intense ion cyclotron wave heating, where minority ions reach energies in the MeV range [5.54]. Similar results have been obtained in TFTR [5.72] and other tokamaks [5.3]. Some tokamak discharges with neutral-beam-injected fast ions have also shown a degree of sawtooth stabilization [5.73, 5.74], although it is difficult to obtain a substantial lengthening of the sawtooth period with neutral beam heating in present experiments. These results are in good agreement with theories of internal kink stabilization by energetic ions [5.52, 5.55, 5.56, 5.75–5.78].

If ITER reaches ignition, fusion alpha particles may be expected to suppress sawteeth transiently, for periods that are long on the energy confinement time scale. Under the assumption that the sawtooth-free period in ITER is limited by the expansion of the q profile as in JET, an extrapolation from the JET results indicates that long-duration monster sawteeth with periods of the order of 100 s are possible in ignited ITER discharges. This conclusion is corroborated by simulations [5.79]. Other numerical MHD codes that include the kinetic effects of the fast particles, as well as those of the thermal ions, are testing these theories [5.80, 5.81]. Although such transient sawtooth suppression may be beneficial in allowing for peaked profiles and an increased ignition margin, the large crashes associated with the long duration periods are a concern. Sawteeth themselves are not able to directly produce any significant electromagnetic or thermal heat load on the plasma facing components or generate a significant fluctuations in the neutron flux but can trigger formation of neoclassical island, big ELM, or other MHD events. As it was observed in experiments, a combination of these perturbations can sometimes trigger a major disruption or a local overheating of the first wall with the following contamination of the plasma by impurities. If it will be necessary for optimization of the plasma performance, a local control of the plasma current profile near q = 1 magnetic surface by ECR or ICR auxiliary systems can be employed to reduce period and magnitude of the sawteeth and hence to mitigate the internal perturbations. It was also shown that application of plasma auxiliary heating and current drive at

the current ramp up phase allows to shape sawteeth free current profile with q(0) > 1 and maintain it for as long as 800 s (see Chapter 6).

5.4.1.3. Fishbone oscillations

Fishbone oscillations were first observed in PDX experiments with nearly perpendicular neutral beam injection [5.59]. The structure of the unstable mode was identified as the $m = 1$, $n = 1$ internal kink mode, with a precursor oscillation frequency close to the thermal ion diamagnetic frequency as well as the fast ion magnetic precessional frequency. Fishbone oscillations were later observed in DIII-D experiments with nearly tangential neutral beam injection and in many other tokamaks worldwide [5.3]. Fishbones were observed to cause severe losses of beam ions in PDX and significant losses in DIII-D, but only minor fast particle redistribution in large tokamaks such as JET, TFTR, and JT-60U.

The first theoretical interpretation [5.58] of the fishbone instability correctly identified the resonant wave particle interaction at the magnetic precession frequency of the trapped fast ions as an essential part of the instability mechanism. Ion diamagnetic effects were subsequently taken into account [5.57]. Eventually a more complete theory emerged that accounts for both collisionless and collisional regimes, the trapped as well as the transit ion response of the fast ions, and finite orbit width corrections [5.52, 5.82, 5.83]. This theory also clarifies the regimes in which fast ions can either stabilize internal kinks or resonantly destabilize them. In particular, a window in parameter space, within which both fishbones and sawteeth are stable, has been identified theoretically [5.52, 5.76, 5.77, 5.83–5.85].

Fusion alpha particles typically have energies such that their magnetic precession frequency is much higher than the thermal ion diamagnetic frequency. In this case, the threshold for the excitation of alpha-driven precessional drift fishbones depends on the alpha particle density [5.52, 5.55]. In the large-aspect-ratio limit, the analytic expression for the threshold is

$$\beta^*_{p\alpha} > \beta^{crit}_{p\alpha} = 0.45 s_1 (\bar{\omega}_{D\alpha} / \omega_A)(R_0 / r_1)^{3/2} \quad (5\text{-}3)$$

where the parameter

$$\beta^*_{p\alpha} = -\frac{8\pi}{B_p^2(r_1)} \int_0^1 dx\, x^{3/2} \frac{dp_\alpha}{dx} \quad , \quad (5\text{-}4)$$

with $x = r/r_1$, depends on the alpha particle pressure within the $q = 1$ surface; here, r_1 is the $q = 1$ radius, and $s_1 = r_1 q'(r_1)$ is the magnetic shear parameter, with $\omega_A = v_A / R_0\sqrt{3}$ and $\bar{\omega}_{D\alpha} = cE_\alpha / 2eB_T r_1 R_0$ (evaluated at birth energy E_α = 3.5 MeV). The instability threshold is somewhat higher when thermal ion Landau damping is taken into account [5.56].

Simulation codes have provided numerical estimates of the fishbone threshold with averaging over the full pitch angle distribution. An analytic study [5.86] for ITER parameters that included the effects of shaping, finite aspect ratio, and finite beta found fishbone instability when the alpha particle beta exceeds 1% on axis, which is only slightly higher than the nominal value expected. Hence, alpha particle-driven fishbone oscillations are a possibility in ITER.

The fishbone-induced particle losses observed experimentally have been simulated with a Monte Carlo code [5.87]. Energetic particle losses occur through a secular outward drift of that fraction of the particles that resonate with the mode. At a larger mode amplitude, stochastic orbit losses become possible. An empirical predator-prey model has been proposed whose predictions are in qualitative agreement with PDX and TFTR results [5.88, 5.89]. The average effect is to keep the alpha particle population close to the value that corresponds to marginal stability. However, more realistic simulations are needed to understand whether the effect of the instability is simply a redistribution of the population or the ejection of a significant fraction of the alpha particles. A model is being developed [5.90, 5.91] to interpret the nonlinear behavior of fishbones, including its experimentally observed frequency chirping. An important parameter is the average width of the trapped banana orbit of the fast ions divided by the plasma minor radius. When this ratio is relatively large, significant losses of the resonant fast ions can be expected, as

was the case in PDX and DIII-D experiments. For smaller widths, the fast ions could be redistributed but remain confined within the plasma, consistent with the observations in present-day large-size tokamaks. If this also occurs in ITER, then it should be relatively safe from alpha particle losses induced by fishbones. A nonperturbative simulation of fishbone oscillations was carried out by concentrating on the wave-particle trapping nonlinearity – and neglecting the fluid wave-wave nonlinearity [5.92]. Even with the neglect of the latter saturation mechanism, fishbone bursts occur with amplitude of plasma displacement no greater than roughly $\xi_\rho/a \sim 0.1$. These bursts produce redistribution but no loss of trapped alphas. The simulations assume that the kink is MHD stable in the absence of alphas, so that an instability exists only for β_{fast} above a threshold value.

5.4.1.4. Kinetic ballooning modes

Resonant excitation of kinetic ballooning modes has been analyzed theoretically [5.61]. Two types of modes may exist. The MHD branch exists only when the tokamak plasma is ideal-MHD unstable. The other branch is the energetic particle continuum mode, with frequency lying in the MHD continuum. The latter can be excited even if the plasma is ideal-MHD stable, but the energetic particle pressure must exceed a threshold. In TFTR, kinetic ballooning modes have been found experimentally to cause loss of alpha particles [5.60], although in ITER it is expected that these modes would likely only cause redistribution.

5.4.1.5. Localized interchange modes

The ideal MHD Mercier criterion for the stability of localized interchange modes [5.93] is easily violated by modest pressure gradients in the plasma region where $q \leq 1$. However, high-m localized interchange modes can be stabilized by finite ion Larmor radius effects, while intermediate-m modes can be suppressed by energetic ions as well as by thermal trapped ions. A

large-aspect-ratio analytic calculation [5.63], in the limit of low central magnetic shear, but with finite elongation of the central flux surfaces, showed that alpha particles can suppress localized interchange modes when their on-axis pressure exceeds 10% of the peak thermal pressure, which is possible for ITER parameters.

5.4.2. Alfvén Frequency Modes

5.4.2.1. Introduction to Alfvén gap eigenmodes

About ten years ago, it was realized that Alfvén modes could be a serious threat to the good classical confinement of energetic alpha-particles in tokamaks and, hence, to the achievement of ignition in a next step device [5.94-5.96]. Since that time a significant progress has been achieved in development of theory and in dedicated experimental study of Alfvén modes in the present machines. The various eigenmodes were observed and identified in experiments and simulated numerically with an impressive degree of details.

Toroidicity causes the continuous frequency spectrum of shear Alfvén waves in a tokamak plasma to exhibit a radial "gap" (analogous to a Brillouin band gap for valence electrons in a periodic crystal lattice). Within this gap can exist discrete-frequency modes, called *toroidal Alfvén eigenmodes* (TAE) [5.94, 5.95]. The frequency gap is centered at $\omega_{TAE}(r) = v_A/2qR$, with v_A the Alfvén speed, q the safety factor, and R the major radius. The gap width is on the order of the inverse aspect ratio, $\Delta\omega/\omega_{TAE} \approx O(r/R)$. Since alpha particles in a thermonuclear plasma have velocities that are typically super-Alfvénic, they can resonantly interact with and destabilize the weakly damped TAE modes [5.96].

In high-temperature plasmas, non-ideal effects such as finite ion Larmor radius and electron collisions can become important in the gap region and cause the Alfvén continuum to split into a series of *kinetic toroidal Alfvén eigenmodes* at closely spaced frequencies above the ideal TAE frequency [5.97–5.100].

In the central region of the plasma, a low-shear version of the TAE mode can arise, called the *core-localized mode* [5.101, 5.102]. Multiple core-localized modes can exist within a single Alfvén gap, for fixed mode number, when the local value of the inverse aspect ratio exceeds that of the magnetic shear [5.103].

Noncircular shaping of the plasma poloidal cross section creates other gaps in the Alfvén continuum, at higher frequencies. Ellipticity creates a gap, at about twice the TAE frequency, within which exist *ellipticity-induced Alfvén eigenmodes*, and similarly for the *triangularity-induced Alfvén eigenmodes* at three times the TAE frequency [5.104].

The ideal and kinetic TAE, as well as the ellipticity and triangularity Alfvén eigenmodes, are "cavity" modes, whose frequencies are determined by the bulk plasma. In addition, a "beam" mode can arise that is not a natural eigenmode of the plasma, but is supported by the presence of a population of energetic particles — and also destabilized by them. This so-called *energetic particle mode* [5.105], which can also exist outside the TAE gap, has a frequency related to the toroidal precessional frequency and poloidal transit/bounce frequency of the fast ions.

The schematic in Fig. 5-7 illustrates these various modes. Shown are radial plots of shear Alfvén continuum curves, with a toroidicity-induced gap that extends radially across the plasma, as well as ellipticity and triangularity gaps at higher frequencies. Straight horizontal lines are heuristically drawn to indicate the typical frequency, mode location, and mode width for the various kinds of modes.

5.4.2.2. Review of Alfvén eigenmode experimental results

Much recent experimental work has been performed on Alfvén-frequency collective instabilities excited by energetic ions [5.3]. Each of the instabilities of interest has been observed to be excited by neutral beam fast ions or ion cyclotron wave-heated tail ions, and some have also been seen with alpha particles.

The most serious instability for ITER seems to be the toroidicity-induced Alfvén eigenmode (TAE), which has caused up to ≈70% loss of injected fast beam ions in the TFTR [5.71] and DIII-D tokamaks [5.106–5.109], albeit only when the toroidal field was lowered to make the neutral beam ions nearly super-Alfvénic. An example of TAE-induced fast ion loss in DIII-D is shown in Fig. 5-8. Multiple TAE modes were observed with $n \approx$ 3-8, separated in frequency by a small Doppler shift due to toroidal rotation. The threshold for TAE instability with neutral beam ions was typically $\langle \beta_f \rangle \approx 1\%$, somewhat larger than the alpha particle beta value expected in ITER (see Table 5-I).

In ITER the most unstable alpha-driven TAE modes are expected to have high toroidal mode numbers, implying the possibility of many small-scale TAE modes, with typical frequency near $f \approx 100$ kHz. The level of the internal electron density and external magnetic fluctuations due to TAEs would probably be similar to that in present neutral beam and ion cyclotron heating simulation experiments, i.e., $\delta n / n \approx 0.1$–1.0% and $\delta B / B_T \approx 10^{-6}$–$10^{-5}$. The saturation levels of TAEs and their effects on alpha particle transport are generally difficult to predict, since these two phenomena are nonlinearly coupled to each other; however, in DIII-D the TAE-induced beam ion loss appeared to control the nonlinear saturation of the TAE instability [5.110].

TAEs are also commonly observed with hydrogen-minority energetic tail ions due to ion cyclotron resonant heating in TFTR [5.111–5.113], JT-60U [5.114–5.116], and JET [5.117]. In TFTR, TAE modes with toroidal mode numbers $n \approx$ 5-8 are produced when the ion cyclotron heating power is above ≈4 MW, with a TAE fast ion beta threshold and frequency spectrum roughly consistent with code modeling. In JT-60U, during second harmonic ion cyclotron minority heating, the number of TAE modes increases with plasma current, so that nine TAE modes are observed at $I_p = 4$ MA, where the maximum toroidal mode number is estimated to be at least $n = 13$. The TAEs in JT-60U were also destabilized by hydrogen minority tail ions with an energy of several MeV, and the TAE threshold of $\langle \beta_f \rangle \approx 0.05\%$ agrees to within a factor of three with code predictions. These TAEs in JT-60U expelled up to 70% of the fast ions with energy above 2.5 MeV from the plasma, with the MeV ion loss increasing linearly with the mode

amplitude. Interestingly, the TAE mode amplitude increased with toroidal mode number. Also, JT-60U demonstrated that current profile control could be effective to control TAE modes.

Recent JT-60U experiments with ion cyclotron heated fast tail ions showed not only TAE modes, but also the higher frequency Alfvén eigenmodes induced by ellipticity and triangularity [5.118]. These modes all exhibited significant downshifting of the frequency (hence the name "tornado" modes) and were correlated with noticeable decreases in the neutron signal, indicating fast ion loss [5.119]. Unstable ellipticity- and triangularity-induced Alfvén modes have also been observed in ion cyclotron wave-heated fast ion experiments on JET [5.120, 5.121]. Curiously, the ellipticity Alfvén eigenmode has even been observed in circular-cross-section plasmas in TFTR with ion cyclotron heating [5.122], probably due to trapped fast ion pressure anisotropy.

The first observation of TAEs purely driven by alpha particles was made in TFTR deuterium-tritium experiments, but only in discharges with high $q(0)$ and weak magnetic shear, and only after (≈100 ms) the neutral beam heating was turned off [5.123]. These conditions were consistent with predictions for the transient excitation of core-localized TAEs. In this special regime the alpha particle beta threshold for these modes was as low as $\beta_\alpha(0) \approx 1\text{-}2 \times 10^{-4}$, i.e., about 50 times lower than the expected value for ITER. The mode amplitudes were very low, as illustrated in Fig. 5-9, and no TAE-induced alpha particle loss was observed, although the alpha particles were apparently redistributed radially outward [5.124]. No TAEs were observed during low-$q(0)$ discharges even at much higher alpha particle beta values (by about a factor of ten), indicating the sensitivity of the TAE instability to the q(r) profile.

Experimental evidence of core-localized TAE modes excited by fast ions from ion cyclotron heating has been found in TFTR [5.125] and in a weakly shear-reversed discharge in JT-60U [5.126]. In the JT-60U experiments, if the discharge was strongly shear-reversed, TAE activity was not observed until the internal transport barrier partially relaxed, reducing the central plasma density. Core-localized TAE modes have also been observed in the START spherical tokamak [5.127], which has a flat central q(r) profile due to its tight aspect ratio configuration.

Both ideal and kinetic TAE modes have been actively excited in JET in an ohmic plasma (without any energetic ions) by the use of external antennas, and their frequency and damping rate directly measured with passive antennas [5.120, 5.128]. Excellent agreement between the observed and predicted TAE frequencies was obtained for these externally launched TAEs. In these antenna experiments, it was also noticed that the formation of an X-point stabilizes low-*n* TAE modes, probably due to increased shear [5.129].

Several other types of collective fast particle effects have also been observed during heating experiments with beam ions or ion cyclotron wave-heated tail ions. In DIII-D at high normalized beta, the frequency of the dominant neutral beam fast ion-driven TAE mode was found to drop abruptly by a factor of two, but still continue to scale with the Alfven frequency, suggesting a transition to a new "beta-induced" Alfvén eigenmode [5.130]. In TFTR in relatively low $q(a)$ discharges, a new branch of the ion cyclotron heated H-minority driven TAE mode was observed [5.131], with a somewhat lower frequency and a more global mode structure than the previously identified TAE peaks.

The TAE mode has also been seen in the W7-AS stellarator [5.132] and the CHS heliotron/torsatron [5.133] for discharges with finite magnetic shear, excited by neutral beam ions. When W7-AS was operated with zero magnetic shear, a Global Alfvén Eigenmode was instead observed [5.134].

5.4.2.3. Linear stability thresholds in ITER

The stability of the various Alfvén modes depends on the competition between the alpha particle pressure-gradient drive and dissipative mechanisms such as continuum [5.135–5.138] and radiative damping [5.97], ion Landau damping [5.139] (for both thermal and fast ions), electron Landau damping [5.140], and trapped electron collisional damping [5.141, 5.142]. For modes with low to moderate toroidal mode numbers, typically ion Landau damping is dominant, whereas for high-*n* modes the trapped electron collisional damping and radiative damping are strong

stabilizing mechanisms. Because ion Landau damping is exponentially sensitive to the thermal ion beta value, the demarcation of regimes for TAE stability in a tokamak reactor is somewhat approximate. Too, as the orbit width of the alpha particles increases, their destabilizing effect tends to be mitigated. The linear instability drive increases linearly with the toroidal mode number *n* until the orbit width becomes comparable to the TAE mode width, at which point the drive becomes independent of the mode number [5.143]. When the orbit width exceeds the poloidal mode wavelength, the drive is predicted to decrease with mode number [5.99, 5.142].

Various numerical codes were developed to interpret the Alfvén eigenmodes observed in fast ion experiments on present large tokamaks. For example, the GATO and CONT codes were used to analyze TAE and beta-induced Alfvén eigenmode experiments in DIII-D [5.144]. The CASTOR global antenna code [5.145, 5.146] and the PENN finite element code [5.147] were used to calculate the TAE, kinetic TAE, ellipticity Alfvén eigenmode, and core-localized TAE spectra and eigenfunctions for shaped equilibria in the external antenna excitation experiments on JET without fast particles. The CASTOR-K hybrid kinetic code analyzed TAE modes in JET deuterium-tritium discharges [5.148]. The NOVA-K kinetic-MHD hybrid stability code [5.149-5.151] and the Landau-gyrofluid initial value code TAE/FL [5.152] were used extensively to analyze TFTR stability. The NOVA-K code was also applied to study TAE stability in JT-60U with ion cyclotron resonant heating [5.153], as well as in a proposed JT-60 Super Upgrade device with very high energy (0.5 MeV) negative-ion neutral beam injection [5.154]. Many more instances of theory, code, and experimental interplay could be cited. In general, the theoretical frequencies and mode structure have been found to match the experimental measurements quite well, while the stability thresholds, more difficult to calculate, are in reasonable agreement.

In particular, the stability of ITER with respect to TAE modes has been examined. The stability predictions are also rather sensitive to the equilibrium profiles, in particular, the safety factor profile and the energetic particle distribution. For normal high-current operation, two classes of ITER-specific equilibrium profiles have been obtained from the PRETOR and TRANSP transport codes [5.70, 5.155]. One class has density and safety factor profiles for ITER that are

characteristic of post-sawtooth behavior — i.e., nearly flat out to the sawtooth inversion radius, which is rather large, at least half the minor radius. Another class of profiles are more peaked; these would be consistent with the expectation that fusion alpha particles suppress sawteeth for long periods in ITER.

A large-aspect-ratio stability code [5.156] found that flattish equilibrium profiles generated by the PRETOR transport code would be unstable for toroidal mode numbers in the range $6 < n < 60$; these results were useful in focusing attention on the issue of high-mode-number stability [5.156]. A single-Alfvén-gap local analysis examined whether the ignition curves for ITER, with helium recycling taken into account, would intersect the $m = n = 10$ TAE instability boundaries [5.157]. Calculations done with the NOVA-K code have indicated [5.158] that PRETOR-type flat profiles are in fact stable for $n \leq 10$ (and possibly higher) — but that more peaked profiles are unstable for $n \geq 12$. Plasma cross-section shaping, i.e., varying the ellipticity and triangularity while fixing the aspect ratio, minor radius, and pressure and safety factor profiles, tends to reduce TAE instability [5.159]. Simulations with the TAE/FL code also found that the PRETOR-type flat profiles for ITER are stable, up to $n = 20$. With the CASTOR-K code, it was found that for a peaked alpha particle pressure profile, kinetic TAE modes in the upper continuum with $n > 10$ can be unstable [5.160, 5.161].

The most unstable type of TAE mode in ITER is likely the core-localized version, whose growth rate tends to be stronger that of the usual TAE modes. This mode can occur in the low-shear central region of the plasma, which is where destabilizing alpha particles are plentiful, and it can also arise near a shear-reversal point of a high-$q(0)$ plasma configuration. Numerical simulations [5.4, 5.158] including ion Landau damping found that the $n = 15$ core-localized TAE mode in ITER can be unstable, nearly independent of temperature, when the peak plasma density is less than 10^{20} m^{-3} (see Fig. 5-10).

Thus, although the stability predictions are sensitive to details of the equilibrium profiles, in general the code results as well as theoretical estimates all indicate that the stability of high-n TAE modes ($n > 10$) is the critical issue for large-size devices like ITER.

Accordingly, high-*n* global codes have been developed that can analyze the full two-dimensional eigenmode structure for equilibria specific to the ITER configuration. The HINT high-*n* code [5.162] and the 2DWKB code [5.163] are based on a WKB (i.e., ballooning-type) formalism; a more recent version of the former code [5.164] uses instead a double Fourier transform representation. These codes include a full kinetic description for the dynamics of the energetic alpha particles and, hence, are computationally demanding. For a typical ITER-like scenario, it was found [5.165] that the mode structure is a mixture of ideal and kinetic TAE modes. The mode frequency is shifted toward the lower Alfvén continuum [5.166] by finite-beta effects [5.167, 5.168], so that radiative damping is enhanced, and the TAE modes tend to be stable. At the same time, energetic particle continuum modes can be excited from the Alfvén continuum below the TAE gap if the energetic particle pressure exceeds a threshold. However, the ITER reference scenario is probably stable with respect to the continuum modes, although not strongly so — Fig. 5-11 indicates that, for instability, the beta value of the alpha particles needs to be only about 25% larger than its nominal ITER value.

The DIII-D observation of beta-induced Alfvén eigenmodes in the ion diamagnetic frequency range, associated with appreciate fast particle losses, motivated a study of the relationship of these modes with kinetic ballooning modes [5.62], which showed that they are two distinct branches of the low-frequency shear Alfvén wave. The most unstable scenario is predicted to occur when thermal ion transit frequency and ion diamagnetic frequency are approximately equal, corresponding to a strong coupling between the two branches due to finite thermal ion temperature gradient. An alternative explanation for the beta-induced Alfvén mode is that it is a natural eigenmode lying in a frequency gap caused by the compressibility of the magnetosonic branch, below the TAE gap [5.130].

Because recent experiments in JT-60U with ion cyclotron heated fast ions have indicated the possibility of suppressing TAE instability by control of the toroidal rotation velocity [5.116], rotational effects are now being incorporated into some stability calculations. One computation [5.169] predicts that stabilization would require a sheared poloidal flow on the order of one-third

the acoustic speed, probably too large to be achieved in ITER. Also, theory has shown that fusion alpha particles in a tokamak reactor will not themselves be able to drive plasma rotation that is sufficiently large to help avoid MHD instabilities or to generate enough rotational shear to suppress turbulence [5.170].

5.4.2.4. Nonlinear behavior and anomalous transport

With the alpha particles in ITER supplying 300 MW of heating power, of which the loss of even only a small fraction could lead to significant wall loading, it is important to consider alpha particle transport due to collective effects and investigate the heat deposition profile. Two main physical mechanisms that have been studied for the nonlinear TAE behavior are kinetic wave-particle trapping and fluid mode-mode coupling.

Initial estimates of TAE-induced resonant alpha particle losses were obtained from test-particle simulations in full toroidal geometry with externally imposed TAE modes [5.171]. This motivated the development of self-consistent theories that allowed the wave amplitudes to evolve, which showed that saturation occurs due to the redistribution of resonant particles by finite amplitude waves [5.172]. This saturation mechanism for TAE modes was confirmed with Lagrangian-type codes [5.173–5.175], an MHD-gyrokinetic hybrid code [5.176], and an MHD-Vlasov code [5.177].

When the continuous creation of fusion-product alpha particles in an ignited plasma, as well as the effects of background damping and collisional relaxation of the alpha particles, are taken into account, wave energy pulsations are found, rather than steady-state saturation [5.178, 5.179]. The dissipation causes the saturated fields to decay until the fusion source reconstitutes the alpha particle distribution function, leading to “bursting.” This behavior resembles the experimental observations of periodic expulsions of fast ions in DIII-D and TFTR neutral beam experiments.

Near the marginal stability threshold for the mode, where the saturation time is much shorter than the trapped particle bounce period, other types of nonlinear behavior can occur [5.180]. A detailed analysis of TFTR was done near marginal stability [5.181, 5.182]. which is the natural situation for experiments in which the fast ion population builds up slowly compared to the mode growth time scale. An interesting situation when the mode is barely above threshold is that its amplitude can grow explosively and persist for several hundred inverse growth times, while its frequency meanwhile bifurcates and shifts both upward and downward significantly; theory and simulations have explained this phenomena as the formation of a phase space structure consisting of a hole-and-clump pair [5.183]. This theory may be relevant to the interpretation of fast particle-excited modes with strong frequency chirping observed in the CHS torsatron; in the START spherical tokamak; in the TFTR, DIII-D, JT-60U, and JET tokamaks; and (with energetic electrons) in the Terella magnetic dipole device [5.90].

As long as the particle resonances do not overlap, the nonlinear oscillations are benign in the sense of not causing appreciable particle loss or change of the alpha particle heating profile. However, if mode overlap occurs because the saturation level is high enough or because multiple modes become unstable, then the alpha particle distribution can change significantly, with a substantial amount of the free energy of the energetic particles being rapidly converted to wave energy. For instance, a subset of modes can flatten over overlapping resonances and provide a seed to trigger a “domino” avalanche (see Fig. 5-12), leading to global mode overlap and, consequently, anomalous radial diffusion and alpha particle loss [5.184].

Transport of alpha particles resonantly interacting with a realistic set of ten strongly unstable core-localized TAE modes was studied with the FAC code specifically for ITER parameters [5.185]. The alpha particles were found to be moved outwards, with their time-evolved distribution locally flattening, but the density profile modification is minimal and no alpha particles are lost (see Fig. 5-13). This result suggests that redistribution of alpha or other energetic particles may possibly be much smaller in ITER than in current tokamaks. It should be kept in mind, however, that the CASTOR-K code, used to generate the linear mode structures for these

calculations, had difficulty (due to strong continuum/radiative damping) in finding unstable modes unless the equilibrium q-profile was sensitively adjusted.

Other nonlinear mechanisms have also been investigated. In mode-mode coupling, saturation occurs due to nonlinear distortion of the mode structure, which dissipates energy on very short spatial scales [5.186–5.188]. This is important for cases of strong instability drive or when the modes are near the ideal continuum. Another fluid-type nonlinear saturation mechanism is the generation of $m = 0$, $n = 0$ velocity shear by angular momentum transfer [5.189]. An alliterative mode-mode coupling explanation for TAE nonlinear saturation has been based on ion Compton scattering, in which the nonlinear $J \times B$ force transfers energy from the TAE waves, to be damped through ion sound waves [5.190, 5.191]. Also, the energetic particle continuum modes were seen, in a gyrokinetic simulation, to saturate by resonant particle ejection due to their large amplitude [5.192].

5.5. POSSIBLE ALPHA PARTICLE CONTROL TECHNIQUES

Several ideas have been proposed for the control of alpha particles in various situations. One such context is the concern to prevent helium “ash” (i.e., thermalized alpha particles) from accumulating in a fusion plasma and eventually quenching ignition. Frequency sweeping is a method that may allow energy-selective transport of alpha particles [5.193, 5.194]. When the alpha particles interact with a wave whose frequency is swept, drift orbit islands are created, which can act like “rising buckets” to convectively transport particles radially. Low-n magnetic perturbations are required, with frequencies up to a few hundred kHz, so they can resonate with the alpha particle toroidal precessional frequency. This technique has possible applications not only to helium ash removal, but also to profile control, production of current, and alpha particle channeling. Since neutral beam penetration in ITER will be limited, this method, operated in reverse, might be helpful for fueling at the plasma center. An antenna system with tunable frequency or ion-cyclotron-resonance-heating beat waves, such as has been used for driving TAE

modes externally, could be employed to investigate this frequency-sweeping scheme. Another idea for easing the problem of helium ash accumulation is that low-frequency fishbone instabilities may cause resonant transport and loss of slowed-down alpha particles with energies in the epithermal range (200-400 keV). Here, the relevant wave-particle resonance involves the precession frequency of the slowed-down alphas and the thermal ion diamagnetic frequency [5.195].

Alpha particle "channeling" is a scheme for transferring the energy of fusion-product alpha particles directly to plasma ions through various waves, thus avoiding the inefficient intermediate step of slowing down on thermal electrons [5.196]. Some recent experiments on TFTR have indicated that the reverse of this process — viz., energy transfer to beam ions by radio-frequency wave heating — may occur, although the corresponding interaction with alpha particles is not yet observed [5.197, 5.198]. Frequency sweeping with a coherent mode can enhance the transfer of free energy from alpha particles to a wave [5.199] and thus help achieve channeling. If channeling can be made to work, it could lead to a compact and efficient tokamak reactor, albeit a next-generation device after ITER.

Finally, it is possible that ion cyclotron emission — viz., emission at ion cyclotron frequencies near the plasma edge, driven by highly energetic fusion-product particles, which has been observed in JET, TFTR, and JT-60U experiments [5.200–5.207] — could be useful for diagnosing certain information about fast ions or edge plasma conditions, or for studying alpha particle channeling.

5.6. CONCLUDING REMARKS

The understanding of the special physical behavior of alpha particles has significantly advanced in recent years, due to new theoretical models, powerful simulation codes, and numerous fast particle experiments, all of which have benefited from extensive interaction. ITER has actually helped stimulate this advance in understanding by focusing attention on issues, many previously unexplored, that are of concern for a large-scale burning plasma.

Experimentally, the alpha particle physics of ITER has been tested to some extent with the use of fast ions in existing tokamak experiments. Direct extrapolations from the behavior in present-day fast ion experiments to that in ITER are possible only within a limited range, since the values of the characteristic dimensionless parameters are quite different.

Calculations of toroidal field ripple loss, which are very accurate, show that the single-particle confinement of energetic alpha particles in ITER is satisfactory.

Theoretical models and simulations of collective effects indicate that a spectrum of modes, especially with high mode numbers (due to ITER's large size), may be unstable, although ion density background damping and separatrix effects are stabilizing. Alpha particles could also possibly excite low-frequency MHD modes such as the fishbone; however, they may suppress sawteeth oscillations transiently. Calculations of anomalous loss due to instabilities are beginning to provide some predictions for ITER. Unless unstable modes overlap and extend to the wall, nonlinear redistribution of alpha particles may merely cause internal profile broadening, without much actual loss.

Although reliable theoretical predictions of instability-induced alpha particle loss are not yet complete and experimental conditions of present-day machines are too far from those of ITER, it is possible to estimate the anomalous loss for two limiting cases. (1) *Single-event abrupt loss*: Assume that all of the high-energy alpha particles are suddenly lost from the plasma core in a single event, after which the alpha confinement is restored. Modeling the power balance for this scenario shows that the alpha particle pressure and hence the heating of the main plasma are restored after a few hundred milliseconds (since $t \approx \tau_s \approx 0.5\,\mathrm{sec} << \tau_E \approx 5\,\mathrm{sec}$), before the plasma cools down due to heat loss. Hence ignition in ITER is not lost. Also, because the mean free path of alpha particles in the material of the first wall is small, heat loading during this type of abrupt alpha particle loss event will evaporate only a thin layer of beryllium armor at the hot spots, which is probably acceptable as long as these events are not very frequent. To estimate the effect of the bursts on the life time of the plasma facing components, more modeling and experimental study of this kind of loss, especially its peaking factor, would be useful. (2) *Diffusive loss*: Present-day

experiments show that in a quiescent plasma, the diffusion rate of the fast particles is close to the neoclassical level. This would not lead to any noticeable loss in ITER. Even if one considers the case when anomalous diffusion by the fast alpha particles is at a rate nearly the same as that predicted by empirical scaling for the particles in the main plasma, estimates show that the energy loss fraction will be less than the ITER design specification of 5%.

In view of the energetic ion results to date, the general conclusion is that the nominal alpha confinement in ITER should be good enough to provide efficient alpha particle heating. However, it is prudent to expect that there will be a small level of alpha loss due to toroidal field ripple in ITER, and that alpha-driven TAE or other collective instabilities may occasionally expel a larger fraction of the alpha particles from the plasma. Therefore the ITER first-wall protection and cooling systems should be designed to withstand a steady-state alpha loss of a few percent, as well as occasional off-normal events. Investigating new techniques for early detection and avoidance of such instabilities in ITER would be worthwhile.

Not all alpha-particle effects, which are potentially important for the plasma performance in ITER, have been discussed in this review. For example, one can expect that energetic particles might affect formation of neoclassical islands which are believed to be the major beta-limiting phenomena in ITER (see Chapter 3). Both theoretical and experimental studies are needed to quantify the effect in ITER type plasmas. It is also not clear what will be energetic particle effect on ELMs frequency and magnitude and on the edge temperature pedestal in ITER. It is well established now that the edge parameters have a strong impact on the core plasma parameters (see Chapter 2) and, therefore, theoretical and experimental studies of energetic particle effects on the edge would be very important for optimization of plasma performance in ITER.

In conclusion, the physics of energetic ions will be an exciting research area for ITER, since it will be the first fusion experiment to explore the behavior of alpha particles in a self-sustained burning plasma. Valuable information has been obtained from the TFTR and JET deuterium-tritium experiments, and more understanding can be derived from its analysis. ITER, however, will fully enter the new regime in which high-energy alpha particles are copiously

produced and the plasma heats itself. Studying the properties of instabilities such as Alfvén eigenmodes and fishbones and their associated anomalous transport, inventing operating techniques to control or mitigate their consequences, exploring how to reduce ripple loss (especially when the plasma operates in shear-optimized advanced modes), designing observational diagnostics appropriate for the harsh environment of a burning plasma — these are all important science issues that can be properly addressed in a burning plasma experiment like ITER.

REFERENCES

[5.1] KOLESNICHENKO, Y. I., Nucl. Fusion 20 (1980) 727.

[5.2] FURTH, H. P., GOLDSTON, R. J., ZWEBEN, S. J., SIGMAR, D. J., Nucl. Fusion 30 (1990) 1799.

[5.3] HEIDBRINK, W. W., SADLER, G. J., Nucl. Fusion 34 (1994) 535.

[5.4] CHENG, C. Z., et al., in Fusion Energy 1996 (Proc. 16th Int. Conf. Montréal, 1996), Vol. 2, IAEA, Vienna (1997) 953.

[5.5] PUTVINSKI, S., et al., in Plasma Physics and Controlled Nuclear Fusion Research 1994 (Proc. 15th Int. Conf. Seville, 1994), Vol. 2, IAEA, Vienna (1995) 535.

[5.6] SPITZER, L., Physics of fully ionized gasses, Interscience Publishers, Inc., New York, 1956.

[5.7] SIVUKHIN, D.V., Coulomb collisions in a fully ionized plasma in Review of Plasma Physics (Consulation Bureau, New York, 1966) Vol;. 4, p.88.

[5.8] STIX, T.H., Plasma Physics 14 (1972) 367.

[5.9] OTT, W., Neutral beam modulation for heating profile measurements, Laboratory Report IPP4/276, Max-Planck Insitute for Plasmaphysik, May 1997.

[5.10] TAYLOR, G., STRACHAN, J. D., BUDNY, R. V., ERNST, D. R., Phys. Rev. Lett. 76 (1996) 2722.

[5.11] THOMAS, P.R., et. al., Phys. Rev. Letters, 80 (1998) 5548.

[5.12] STRACHAN, J. D., et al., Plasma Phys. Contr. Fusion 39 (1997) B103.

[5.13] USHIGUSA, K., et al., in Fusion Energy 1996 (Proc. 16th Int. Conf. Montréal, 1996), Vol. 1, IAEA, Vienna (1997) 37.

[5.14] PETROV, M. P., et al., in Fusion Energy 1996 (Proc. 16th Int. Conf. Montréal, 1996), Vol. 1, IAEA, Vienna (1997) 261.

[5.15] PETROV, M. P., et al., Nucl. Fusion 35 (1995) 1437.

[5.16] UCKAN, N. A., TOLLIVER, J. S., HOULBERG, W. A., ATTENBERGER, S. E., Fusion Technol. 13 (1988) 411.

[5.17] ZWEBEN, S. J., DARROW, D. S., HERRMANN, H. W., BATHA, S. H., BUDNY, R. V., Nucl. Fusion 35 (1995) 893.

[5.18] ZWEBEN, S. J., BOIVIN, R. L., CHANG, C.-S., HAMMETT, G. W., MYNICK, H. E., Nucl. Fusion 31 (1991) 2219.

[5.19] McKEE, G. R., et al., Nucl. Fusion 37 (1997) 501.

[5.20] CONROY, S., JARVIN, O. N., PILLON, M., SADLER, G., in Controlled Fusion and Plasma Physics (Proc. 17th Eur. Conf. Amsterdam, 1990), Vol. 14B, Part I, European Physical Society, Geneva (1990) 98.

[5.21] NISHITANI, T., Plasma Phys. Contr. Fusion 38 (1996) 355.

[5.22] MYRA, J. R., CATTO, P. J., MYNICK, H. E., DUVALL, R. E., Phys. Fluids B 5 (1993) 1160.

[5.23] MANFREDI, G., DENDY, R. O., Phys. Rev. Lett. 76 (1996) 4360.

[5.24] ZWEBEN, S. J., et al., Plasma Phys. Control. Fusion 39 (1997) A275.

[5.25] CATTO, P. J., TESSAROTO, M., Phys. Fluids 31 (1988) 2292.

[5.26] TANI, K., AZUMI, M., DEVOTO, R. S., J. Comp. Phys. 98 (1992) 332.

[5.27] YUSHMANOV, P. N., in Reviews of Plasma Physics, Vol. 16, Consultants Bureau, New York (1990) 117.

[5.28] GOLDSTON, R. J., TOWNER, H. H. J., J. Plasma Phys. 26 (1981) 283.

[5.29] GOLDSTON, R. J., WHITE, R. B., BOOZER, A. H., Phys. Rev. Lett. 47 (1981) 647.

[5.30] SCOTT, S. D., et al., Nucl. Fusion 25 (1985) 359.

[5.31] IKEDA, Y., et al., Nucl. Fusion 36 (1996) 759.

[5.32] TOBITA, K., et al., Phys. Rev. Lett. 69 (1992) 3060.

[5.33] TOBITA, K., et al., in Fusion Energy 1996 (Proc. 16th Int. Conf. Montréal, 1996), Vol. 1, IAEA, Vienna (1997) 497.

[5.34] SADLER, G., et al., Plasma Phys. Control. Fusion 34 (1992) 1971.

[5.35] TUBBING, B. J. D., et al., in Controlled Fusion and Plasma Physics (Proc. 22nd Eur. Conf. Bournemouth, 1995), Vol. 19C, Part IV, European Physical Society, Geneva (1995) 1.

[5.36] PUTVINSKI, S., TUBBING, B. J. D., ERIKSSON, L.-G., KONOVALOV, S. V., Nucl. Fusion 34 (1994) 495.

[5.37] BASIUK, V., et al., Fusion Technol. 26 (1994) 222.

[5.38] WHITE, R. B., BOOZER, A. H., Phys. Plasmas 2 (1995) 2915.

[5.39] KONOVALOV, S. V., TAKIZUKA, T., TANI, K., HAMAMATSU, K., AZUMI, M., “Analysis of High Energy Ion Ripple Loss in the Up-Down Asymmetric Configuration by OFMC Plus Mapping Hybrid Code,” Rep. 94-033, Japan Atomic Energy Research Institute (1994).

[5.40] TOBITA, K., et al., Nucl. Fusion 35 (1995) 1585.

[5.41] GOLDSTON, R. J., JASSBY, D., "Phenomena Accompanying Gradient-B Drift Injection of Energetic Ions into Tokamak Plasmas," Rep. MATT-1244, Princeton Plasma Physics Laboratory (1976).

[5.42] YUSHMANOV, P. N., CARY, J. R., SHASHARINA, S. G., Nucl. Fusion 33 (1993) 1293.

[5.43] REDI, M. H., BUDNY, R. V., McCUNE, D. C., MILLER, C. O., WHITE, R. B., Phys. Plasmas 3 (1996) 3037.

[5.44] DUONG, H. H., et al., Nucl. Fusion 37 (1997) 271.

[5.45] ZWEBEN, S., et al., Nucl. Fusion 35 (1995) 1445.

[5.46] WHITE, R. B., et al., Phys. Plasmas 2 (1995) 2871.

[5.47] RUSKOV, E., et al., "Measurement of Tritium Beam Ion Loss in TFTR Reversed-Shear Plasmas with the Beam-Blip Technique," in Alpha Particles in Fusion Research (Proc. 5th IAEA Tech. Comm. Meeting Abingdon, U.K., 1997), JET Joint Undertaking, Abingdon (1997) 165.

[5.48] ANTONSEN, T. M., LEE, Y. C., Phys. Fluids 25 (1982) 132.

[5.49] VAN DAM, J. W., ROSENBLUTH, M. N., LEE, Y. C., Phys. Fluids 25 (1982) 1349.

[5.50] CONNOR, J. W., HASTIE, R. J., MARTIN, T. J., TURNER, M. F., in Heating in Toroidal Plasmas (Proc. 3rd Joint Varenna-Grenoble Int. Symp. Grenoble, 1982), Vol. 1, CEC, Brussels (1982) 65.

[5.51] ROSENBLUTH, M. N., TSAI, S. T., VAN DAM, J. W., ENGQUIST, M. G., Phys. Rev. Lett. 51 (1983) 1967.

[5.52] PORCELLI, F., Plasma Phys. Contr. Fusion 33 (1991) 1601.

[5.53] HASTIE, R. J., CHEN, Y.-P., KE, F.-J., TSAI, S. T., CHEN, L., Chinese Phys. Lett. 4 (1987) 561.

[5.54] CAMPBELL, D. J., et al., Phys. Rev. Lett. 60 (1988) 2148.

[5.55] COPPI, B., MIGLIUOLO, S., PEGORARO, F., PORCELLI, F., Phys. Fluids B 2 (1990) 927.

[5.56] ROMANELLI, F., CHEN, L., WHITE, R. B., Nucl. Fusion 31 (1991) 631.

[5.57] COPPI, B., PORCELLI, F., Phys. Rev. Lett. 57 (1986) 2272.

[5.58] CHEN, L., WHITE, R. B., ROSENBLUTH, M. N., Phys. Rev. Lett. 52 (1984) 1122.

[5.59] McGUIRE, K., et al., Phys. Rev. Lett. 50 (1983) 891.

[5.60] CHANG, Z., et al., Phys. Rev. Lett. 76 (1996) 1071.

[5.61] TSAI, S. T., CHEN, L., Phys. Fluids B 5 (1993) 3284.

[5.62] ZONCA, F., CHEN, L., SANTORO, R. A., Plasma Phys. Control. Fusion 38 (1996) 2011.

[5.63] PORCELLI, F., ROSENBLUTH, M. N., Plasma Phys. Contr. Fusion 40 (1998) 481.

[5.64] STRATTON, B. C., et al., Nucl. Fusion 36 (1996) 1586.

[5.65] JARVIS, O. N., CONROY, S. W., HONE, M., SADLER, G. J., VAN BELLE, P., in Controlled Fusion and Plasma Physics (Proc. 21st Eur. Conf. Montpellier, France, 1994), Vol. 18B, Part 1, European Physical Society, Geneva (1994) 270.

[5.66] JACQUINOT, J., et al., Fusion Technol. 21 (1992) 2254.

[5.67] MARCUS, F. B., et al., Nucl. Fusion 34 (1994) 687.

[5.68] ODBLOM, A., ANDERSON, D., ERIKSSON, L.-G., LISAK, M., Nucl. Fusion 35 (1995) 1571.

[5.69] KOLESNICHENKO, Y. I., YAKOVENKO, Y. V., Nucl. Fusion 35 (1995) 1579.

[5.70] BUDNY, R. V., MCCUNE, D. C., REDI, M. H., SCHIVELL, J., WIELAND, R. M., Phys. Plasmas 3 (1996) 4583.

[5.71] WONG, K. L., et al., Phys. Rev. Lett. 66 (1991) 1874.

[5.72] HOSEA, J. C., et al., in Plasma Physics and Controlled Nuclear Fusion 1990 (Proc. 13th Int. Conf. Washington, D.C., 1990), Vol. 1, IAEA, Vienna (1991) 669.

[5.73] ONGENA, J., et al., in Controlled Fusion and Plasma Heating (Proc. 17th Eur. Conf. Amsterdam, 1990), Vol. 14B, Part I, European Physical Society, Geneva (1990) 383.

[5.74] NAVE, M. F. F., et al., Nuclear Fusion 31 (1991) 697.

[5.75] COPPI, B., HASTIE, R. J., MIGLIUOLO, S., PEGORARO, F., PORCELLI, F., Phys. Lett. A 132 (1988) 267.

[5.76] COPPI, B., DETRAGIACHE, P., MIGLIUOLO, S., PEGORARO, F., PORCELLI, F., Phys. Rev. Lett. 63 (1989) 2733.

[5.77] WHITE, R. B., BUSSAC, M. N., ROMANELLI, F., Phys. Rev. Lett. 62 (1989) 539.

[5.78] WHITE, R. B., ROMANELLI, F., BUSSAC, M. N., Phys. Fluids B 2 (1990) 745.

[5.79] PORCELLI, F., BOUCHER, D., ROSENBLUTH, M. N., Plasma Phys. Control. Fusion 38 (1996) 2163.

[5.80] ANTONSEN, T. M., BONDESON, A., Phys. Rev. Lett. 71 (1993) 2046.

[5.81] McCLEMENTS, K. G., DENDY, R. O., GIMBLETT, C. G., HASTIE, R. J., MARTIN, T. J., Nucl. Fusion 35 (1995) 1761.

[5.82] PORCELLI, F., STANKIEWICZ, R., BERK, H. L., ZHANG, Y. Z., Phys. Fluids B 4 (1992) 3017.

[5.83] FOGACCIA, G., ROMANELLI, F., Phys. Plasmas 2 (1995) 227.

[5.84] ZHANG, Y. Z., BERK, H. L., MAHAJAN, S. M., Nucl. Fusion 29 (1989) 848.

[5.85] MIGLIUOLO, S., Nucl. Fusion 33 (1993) 1721.

[5.86] WU, Y., CHENG, C. Z., WHITE, R. B., Phys. Plasmas 1 (1994) 3369.

[5.87] WHITE, R. B., GOLDSTON, R. J., McGUIRE, K., BOOZER, A. H., MONTICELLO, D. A., PARK, W., Phys. Fluids 26 (1983) 2958.

[5.88] KAITA, R., et al., Phys. Fluids B 2 (1990) 1584.

[5.89] BORBA, D., NAVE, M. F. F., PORCELLI, F., in Theory of Fusion Plasmas (Proc. Joint Varenna-Lausanne Workshop and Int. School of Plasma Physics, Varenna, Italy, 1992), Editrice Compositori Societa Italiana di Fisica, Bologna (1992) 285.

[5.90] BREIZMAN, B. N., et al., Phys. Plasmas 4 (1997) 1559.

[5.91] CANDY, J., PORCELLI, F., BREIZMAN, B. N., BERK, H. L., in Proceedings of the 24th EPS Conference on Controlled Fusion and Plasma Physics, Berchtesgaden, 1997, Vol. 21A III, European Physical Society, Petit Lancy (1997) 1189.

[5.92] PUTVINSKI, S., et. al., Fusion Energy 1998, (17th Conference Proceedings) IAEA Vienna, 1998.

[5.93] MERCIER, C., Nucl. Fusion 1 (1960) 47.

[5.94] CHENG, C. Z., CHEN, L., CHANCE, M. S., Ann. Phys. (N.Y.) 161 (1985) 21.

[5.95] CHENG, C. Z., CHANCE, M. S., Phys. Fluids 29 (1986) 3695.

[5.96] FU, G. Y., VAN DAM, J. W., Phys. Fluids B 1 (1989) 1949.

[5.97] METT, R. R., MAHAJAN, S. M., Phys. Fluids B 4 (1992) 2885.

[5.98] CANDY, J., ROSENBLUTH, M. N., Phys. Plasmas 1 (1994) 356.

[5.99] BREIZMAN, B. N., SHARAPOV, S., Plasma Phys. Control. Fusion 37 (1995) 1057.

[5.100] BERK, H. L., METT, R. R., LINDBERG, D. M., Phys. Fluids B 5 (1993) 2969.

[5.101] FU, G. Y., Phys. Plasmas 2 (1995) 1029.

[5.102] BERK, H. L., et al., Phys. Plasmas 2 (1995) 3401.

[5.103] CANDY, J., BREIZMAN, B. N., VAN DAM, J. W., OZEKI, T., Phys. Lett. A 215 (1996) 299.

[5.104] BETTI, R., FREIDBERG, J. P., Phys. Fluids B 3 (1991) 1865.

[5.105] CHEN, L., Phys. Plasmas 1 (1994) 1519.

[5.106] HEIDBRINK, W. W., STRAIT, E. J., DOYLE, E., SAGER, G., SNIDER, R. T., Nucl. Fusion 31 (1991) 1635.

[5.107] DUONG, H. H., et al., Nucl. Fusion 33 (1993) 749.

[5.108] STRAIT, E. J., HEIDBRINK, W. W., TURNBULL, A. D., CHU, M. S., DUONG, H. H., Nucl. Fusion 33 (1993) 1849.

[5.109] STRAIT, E. J., HEIDBRINK, W. W., TURNBULL, A. D., Plasma Phys. Cont. Fusion 36 (1994) 1211.

[5.110] HEIDBRINK, W. W., et al., Phys. Fluids B 5 (1993) 2176.

[5.111] WILSON, J. R., et al., in Plasma Physics and Controlled Nuclear Fusion Research 1992 (Proc. 14th Int. Conf. Würzburg, 1992), Vol. 1, IAEA, Vienna (1993) 661.

[5.112] WONG, K. L., et al., Plasma Phys. Control. Fusion 36 (1994) 879.

[5.113] FREDRICKSON, E. D., et al., in Plasma Physics and Controlled Nuclear Fusion Research 1994 (Proc. 15th Int. Conf. Seville, 1994), Vol. 1, IAEA, Vienna (1995) 275.

[5.114] SAIGUSA, M., et al., Plasma Phys. Control. Fusion 37 (1995) 295.

[5.115] KIMURA, H., et al., Phys. Lett. A 199 (1995) 86.

[5.116] KIMURA, H., et al., J. Plasma Fusion Res. 71 (1995) 1147.

[5.117] ALI-ARSHAD, S., CAMPBELL, D. J., Plasma Phys. Contr. Fusion 37 (1995) 715.

[5.118] KRAMER, G. J., et al., "Noncircular Triangularity and Ellipticity Induced Alfvén Eigenmodes Observed in JT-60U," Phys. Rev. Lett. (to be published in vol. 80, no. 12 (1998)).

[5.119] SAIGUSA, M., et al., in TAE Modes and Energetic Particle Physics (Proc. IEA Tripartite Workshop W36 Naka, Japan, 1997), Japan Atomic Energy Research Institute, Naka, Japan (1997) 39.

[5.120] FASOLI, A., et al., Nucl. Fusion 35 (1995) 1485.

[5.121] HEIDBRINK, W. W., FASOLI, A., BORBA, D., JAUN, A., Phys. Plasmas 4 (1997) 3663.

[5.122] FREDRICKSON, E., CHANG, Z., FU, G. Y., in TAE Modes and Energetic Particle Physics (Proc. IEA Tripartite Workshop W36, Naka, Japan, 1997), Japan Atomic Energy Research Institute, Naka, Japan (1997) 327.

[5.123] NAZIKIAN, R., et al., Phys. Rev. Lett. 78 (1997) 2976.

[5.124] PETROV, M., et al., "Experimental Studies of Alpha Particle Radial Density Redistribution in TFTR D-T Plasmas due to Reversed Shear and TAE Modes," in

Alpha Particles in Fusion Research (Proc. 5th IAEA Tech. Comm. Meeting Abingdon, U.K., 1997), JET Joint Undertaking, Abingdon (1997) 161.

[5.125] NAZIKIAN, R., et al., Bull. Am. Phys. Soc. 38 (1993) 1906.

[5.126] KIMURA, H., et al., in Fusion Energy 1996 (Proc. 16th Int. Conf. Montréal, 1996), Vol. 3, IAEA, Vienna (1997) 295.

[5.127] GRYAZNEVICH, M., et al., "Observations of MHD Modes in the Alfvén Frequency Range in Beam-Heated START Discharges," in Alpha Particles in Fusion Research (Proc. 5th IAEA Tech. Comm. Meeting Abingdon, U.K., 1997), JET Joint Undertaking, Abingdon (1997) 53.

[5.128] FASOLI, A., et al., Phys. Rev. Lett. 75 (1995) 645.

[5.129] FASOLI, A., et al., Plasma Phys. Control. Fusion 39 (1997) B287.

[5.130] HEIDBRINK, W. W., STRAIT, E. J., CHU, M. S., TURNBULL, A. D., Phys. Rev. Lett. 71 (1993) 855.

[5.131] FREDRICKSON, et al., Nucl. Fusion 35 (1995) 1457.

[5.132] WELLER, A., et al., "Alfvén Instabilities in WENDELSTEIN 7-AS," in Plasma Phys. Contr. Nucl. Fusion (Proc. 8th Intl. Toki Conf. Toki, Japan, 1997), National Institute for Fusion Science, Toki, Japan (in press).

[5.133] TOI, K., et al., "Global MHD Modes Excited by Energetic Ions in Heliotron/Torsotron Plasmas," in Fusion Energy Research 1998 (Proc. 17th Int. Conf., Yokohama, 1998), paper IAEA-F1-CN-69/EXP1/19 (to be published).

[5.134] WELLER, et al., Phys. Rev. Lett. 72 (1994) 1220.

[5.135] BERK, H. L., VAN DAM, J. W., GUO, Z., LINDBERG, D. M., Phys. Fluids B 4 (1992) 1806.

[5.136] ZONCA, F., CHEN, L., Phys. Rev. Lett. 68 (1992) 592.

[5.137] ROSENBLUTH, M. N., BERK, H. L., VAN DAM, J. W., LINDBERG, D. M., Phys. Rev. Lett. 68 (1992) 596.

[5.138] ROSENBLUTH, M. N., BERK, H. L., VAN DAM, J. W., LINDBERG, D. M., Phys. Fluids B 4 (1992) 2189.

[5.139] BETTI, R., FREIDBERG, J. P., Phys. Fluids B 4 (1992) 1465.

[5.140] CANDY, J., Plasma Phys. Control. Fusion 38 (1996) 795.

[5.141] GORELENKOV, N. N., SHARAPOV, S. E., Phys. Scr. 45 (1992) 163.

[5.142] FU, G. Y., CHENG, C. Z., Phys. Fluids B 4 (1992) 3722.

[5.143] BERK, H. L., BREIZMAN, B. N., YE, H., Phys Lett. A 162 (1992) 475.

[5.144] TURNBULL, A. D., et al., Phys. Fluids B 5 (1993) 2546.

[5.145] POEDTS, S., et al., Plasma Phys. Contr. Fusion 34 (1992) 1397.

[5.146] HUYSMANS, G. T. A., GOEDBLOED, J. P., KERNER, W., Phys. Fluids B 5 (1993) 1545.

[5.147] JAUN, A., APPERT, K., VACLAVIK, J., VILLARD, L., Comput. Phys. Commun. 92 (1995) 153.

[5.148] KERNER, W., et al., "Theory of Alfvén Eigenmode Instabilities and Related Alpha Particle Transport in JET D-T Plasmas," Nucl. Fusion (in press).

[5.149] CHENG, C. Z., et al., in Plasma Physics and Controlled Nuclear Fusion Research 1992 (Proc. 14th Int. Conf. Würzburg, 1992), Vol. 2, IAEA, Vienna (1993) 51.

[5.150] FU, G. Y., et al., Phys. Rev. Lett. 75 (1995) 2336.

[5.151] FU, G. Y., et al., Phys. Plasmas 3 (1996) 4036.

[5.152] SPONG, D. A., HEDRICK, C. L., CARRERAS, B. A., Nucl. Fusion 35 (1995) 1687.

[5.153] FU, G. Y., CHENG, C. Z., KIMURA, H., OZEKI, T., SAIGUSA, M., Nucl. Fusion 36 (1996) 1759.

[5.154] OZEKI, T., CHENG, C. Z., NAGASHIMA, K., Nucl. Fusion 35 (1995) 1553.

[5.155] BOUCHER, D., et al., in Fusion Engineering (Proc. 17th IEEE/NPSS Symposium San Diego, 1997), IEEE, New York Vol 2, p.764 (1997).

[5.156] CANDY, J., ROSENBLUTH, M. N., Nucl. Fusion 35 (1995) 1069.

[5.157] BERK, H. L., et al., in Plasma Physics and Controlled Nuclear Fusion Research 1994 (Proc. 15th Int. Conf. Seville, 1994), Vol. 3, IAEA, Vienna (1995) 547.

[5.158] CHENG, C. Z., et al., in Plasma Physics and Controlled Nuclear Fusion Research 1994 (Proc. 15th Int. Conf. Seville, 1994), Vol. 3, IAEA, Vienna (1996) 373.

[5.159] FU, G. Y., in TAE Modes and Energetic Particle Physics (Proc. IEA Tripartite Workshop W36, Naka, Japan, 1997), Japan Atomic Energy Research Institute, Naka, Japan (1997) 69.

[5.160] BORBA, D., CANDY, J., KERNER, W., SHARAPOV, S., in Theory of Fusion Plasmas (Proc. Int. School of Plasma Physics, Varenna, Italy, 1996), Editrice Compositori Societa Italiana di Fisica, Bologna (1996) 267.

[5.161] BERK, H. L., et al., in Fusion Energy 1996 (Proc. 16th Int. Conf. Montréal, 1996), Vol. 2, International Atomic Energy Agency, Vienna (1997) 439.

[5.162] CHENG, C. Z., GORELENKOV, N. N., HSU, C. T., Nucl. Fusion 35 (1995) 1639.

[5.163] VLAD, G., ZONCA, F., ROMANELLI, F., Nucl. Fusion 35 (1995) 1651.

[5.164] GORELENKOV, N. N., CHENG, C. Z., FU, G. Y., in TAE Modes and Energetic Particle Physics (Proc. IEA Tripartite Workshop W36, Naka, Japan, 1997), Japan Atomic Energy Research Institute, Naka, Japan (1997) 103.

[5.165] ROMANELLI, F., ZONCA, F., in Tokamak Concept Improvement (Proc. Workshop Varenna, 1994), Editrice Compositori Societa Italiana di Fisica, Bologna (1994) 191.

[5.166] SANTORO, R. A., CHEN, L., Phys. Plasmas 3 (1996) 2349.

[5.167] FU, G. Y., CHENG, C. Z., Phys. Fluids B 2 (1990) 985.

[5.168] ZONCA, F., CHEN, L., Phys. Fluids B 5 (1993) 3668.

[5.169] SPONG, D. A., et al., "Alpha-Driven Alfvén Instabilities and Velocity Shear Effects," in Alpha Particles in Fusion Research (Proc. 5th IAEA Tech. Comm. Meeting Abingdon, U.K., 1997), JET Joint Undertaking, Abingdon (1997) 77.

[5.170] ROSENBLUTH, M. N., HINTON, F., Nucl. Fusion 35 (1996) 55.

[5.171] SIGMAR, D. J., HSU, C. T., WHITE, R. B., CHENG, C. Z., Phys. Fluids B 4 (1992) 1506.

[5.172] BERK, H. L., BREIZMAN, B. N., Phys. Fluids B 2 (1990) 2246.

[5.173] BERK, H. L., BREIZMAN, B. N., PEKKER, M., Phys. Plasmas 2 (1995) 3007.

[5.174] BERK, H. L., BREIZMAN, B. N., PEKKER, M. S., Nucl. Fusion 35 (1995) 1713.

[5.175] WU, Y., WHITE, R. B., Phys. Plasmas 1 (1994) 2733.

[5.176] FU, G. Y., PARK, W., Phys. Rev. Lett. 74 (1995) 1594.

[5.177] TODO, Y., SATO, T., WATANABE, K., WATANABE, T. H., HORIUCHI, R., Phys. Plasmas 2 (1995) 2711.

[5.178] BERK, H. L., BREIZMAN, B. N., YE, H., Phys. Rev. Lett. 68 (1992) 3563.

[5.179] BERK, H. L., BREIZMAN, B. N., YE, H., Phys. Fluids B 5 (1993) 3217.

[5.180] BERK, H. L., BREIZMAN, B. N., PEKKER, M., Phys. Rev. Lett. 76 (1996) 1256.

[5.181] WONG, K. L., et al., Phys. Plasmas 4 (1997) 393.

[5.182] BREIZMAN, B. N., BERK, H. L., CANDY, J., PETVIASHVILI, N. V., "Near-Threshold Dynamics of Instabilities Driven by Energetic Particles," in Alpha Particles in Fusion Research (Proc. 5th IAEA Tech. Comm. Meeting Abingdon, U.K., 1997), JET Joint Undertaking, Abingdon (1997) 49.

[5.183] BERK, H. L., BREIZMAN, B. N., PETVIASHVILI, N. V., Phys. Lett. A 234 (1997) 213.

[5.184] BERK, H. L., BREIZMAN, B. N., FITZPATRICK, J., WONG, H. V., Nucl. Fusion 35 (1995) 1661.

[5.185] CANDY, J., BORBA, D. N., BERK, H. L., HUYSMANS, G. T. A., KERNER, W., Phys. Plasmas 4 (1997) 2597.

[5.186] VLAD, G., BRIGUGLIO, S., KAR, C., ZONCA, F., ROMANELLI, F., in Theory of Fusion Plasmas (Proc. Joint Varenna-Lausanne Workshop, Varenna, 1992), Editrice Compositori Societa Italiana di Fisica, Bologna (1992) 361.

[5.187] BRIGUGLIO, S., VLAD, G., ZONCA, F., KAR, C., Phys. Plasmas 2 (1995) 3711.

[5.188] ZONCA, F., ROMANELLI, F., VLAD, G., KAR, C., Phys. Rev. Lett. 74 (1995) 698.

[5.189] SPONG, D. A., CARRERAS, B. A., HEDRICK, C. L., Phys. Plasmas 1 (1994) 1503.

[5.190] GANG, F., Phys. Fluids B 4 (1992) 3152.

[5.191] HAHM, T. S., CHEN, L., Phys. Rev. Lett. 74 (1995) 266.

[5.192] BRIGUGLIO, S., et al., in Fusion Energy 1996 (Proc. 16th Int. Conf. Montréal, 1996), Vol. 2, IAEA, Vienna (1997) 543.

[5.193] MYNICK, H., POMPHREY, N., Nucl. Fusion 34 (1994) 1277.

[5.194] HSU, C. T., CHENG, C. Z., HELANDER, P., SIGMAR, D. J., WHITE, R., Phys. Rev. Lett. 72 (1994) 2503.

[5.195] COPPI, B., PORCELLI, F., Fusion Technol. 13 (1988) 447.

[5.196] FISCH, N. J., RAX, J. M., Phys. Rev. Lett. 69 (1992) 612.

[5.197] DARROW, D. S., et al., Nucl. Fusion 36 (1996) 509.

[5.198] FISCH, N. J., et al., in Fusion Energy 1996 (Proc. 16th Int. Conf. Montréal, 1996), Vol. 1, IAEA, Vienna (1997) 271.

[5.199] BERK, H. L., BREIZMAN, B. N., Comments Plasma Phys. Controlled Fusion 17 (1996) 129.

[5.200] COTTRELL, G. A., DENDY, R. O., Phys. Rev. Lett. 60 (1988) 33.

[5.201] COPPI, B., Phys. Lett. A 172 (1993) 439.

[5.202] CAUFFMAN, S., MAJESKI, R., Rev. Sci. Instrum. 66 (1995) 817.

[5.203] DENDY, R. O., et al., Nucl. Fusion 35 (1995) 1733.

[5.204] BELIKOV, V. S., KOLESNICHENKO, Y. I., SILIVRA, O. A., Nucl. Fusion 35 (1995) 1603.

[5.205] GORELENKOV, N. N., CHENG, C. Z., Nucl. Fusion 35 (1995) 1743.

[5.206] ARUNASALAM, V., J. Plasma Phys. 57 (1997) 523.

[5.207] DA COSTA, O., et al., in TAE Modes and Energetic Particle Physics (Proc. IEA Tripartite Workshop W36, Naka, Japan, 1997), Japan Atomic Energy Research Institute, Naka, Japan (1997) 295.

LIST OF TABLES

LIST OF FIGURES

FIG. 5-9. Observation of alpha-driven TAE modes in TFTR (from Ref. [5.123]). The TAE modes appear ≈150 msec after the end of NBI in DT discharges with high q(0), consistent with theory in which the NBI ions damp the mode and the high q(0) increases the alpha particle drive. The amplitude of these external magnetic perturbations is several orders of magnitude smaller than the usual low frequency MHD modes in TFTR, so there was no perceptible alpha loss associated with these TAE modes.

FIG. 5-10. Stability boundary in the $n_e(0)$-T(0) POPCON diagram for an n = 15 core-localized TAE mode in an ITER-type plasma (from Ref. [5.158]).

FIG. 5-11. Growth rate for the energetic particle-driven continuum mode as a function of the alpha particle beta value (normalized to the ITER reference value) for various toroidal mode numbers. (From Ref. [5.165])

FIG. 5-12. Time evolution of (a) resonance widths for a multi-mode system and (b) resonant particle distribution function, where mode overlap leads to a “domino” avalanche and global diffusion of alpha particles. (From Ref. [5.184])

FIG. 5-13. Anomalous diffusion of the alpha particle distribution caused by 10 strongly unstable core-localized TAE modes in ITER. (From Ref. [5.185])

Table 5-I. Fast Ion Parameters For Various Tokamak Heating Systems.

Parameter	NBI (TFTR)[a]	ICRH JET[b]	Alphas (TFTR)[a]	Alphas (JET) Hot-ion mode[c]	Alphas (JET) Shear-optimized[d]	Alphas (ITER)
$P_f(0)$ [MW/m^3]	3	1–3	0.3	0.12	0.13	0.3
δ / a [e]	0.05	0.3	0.3	0.36	0.35	0.05
$n_f(0) / n_e(0)$ [%]	13	1-10	0.3	0.44	0.34	0.3
$\beta_f(0)$ [%]	0.9	1-3	0.26	0.7	0.44	0.7
$\langle \beta_f \rangle$ [%]	0.4	0.5	0.03	0.12	0.07	0.2
$\max \lvert R \nabla \beta_f \rvert$	0.04	≈ 0.1	0.02	0.035	0.033	0.06
$v_f / v_A(0)$	0.35	$\approx$ 1-2	1.6	1.67	1.4	1.9

Notes:
(a) TFTR with 40 MW of 100 keV NBI in a D-T plasma, B_T = 5 T (discharge #76770).
(b) JET with ≈15 MW of ICRH ^{3}He minority heating with $\langle E_f \rangle \approx 1$ MeV.
(c) Provisional parameters for JET high fusion power (16.1 MW) H-mode hot-ion D-T plasma with $n_T(0):n_D(0)$ = 60:40, B_T = 3.6 T, 22 MW of NBI, and 3.1 MW of ICRH (discharge #42976).
(d) Provisional parameters for JET high fusion power (8 MW) shear-optimized D-T plasma with $n_T(0):n_D(0)$ = 29:71, B_T = 3.45 T, 18 MW of NBI, and 2 MW of ICRH (discharge #42746).
(e) Orbit shift from magnetic flux surface: $\delta = q(R/r)^{1/2}\rho_f$, where ρ_f is the fast particle Larmor radius (for the toroidal magnetic field). Note that $\delta \approx 5\,\rho_f$ at q = 2.

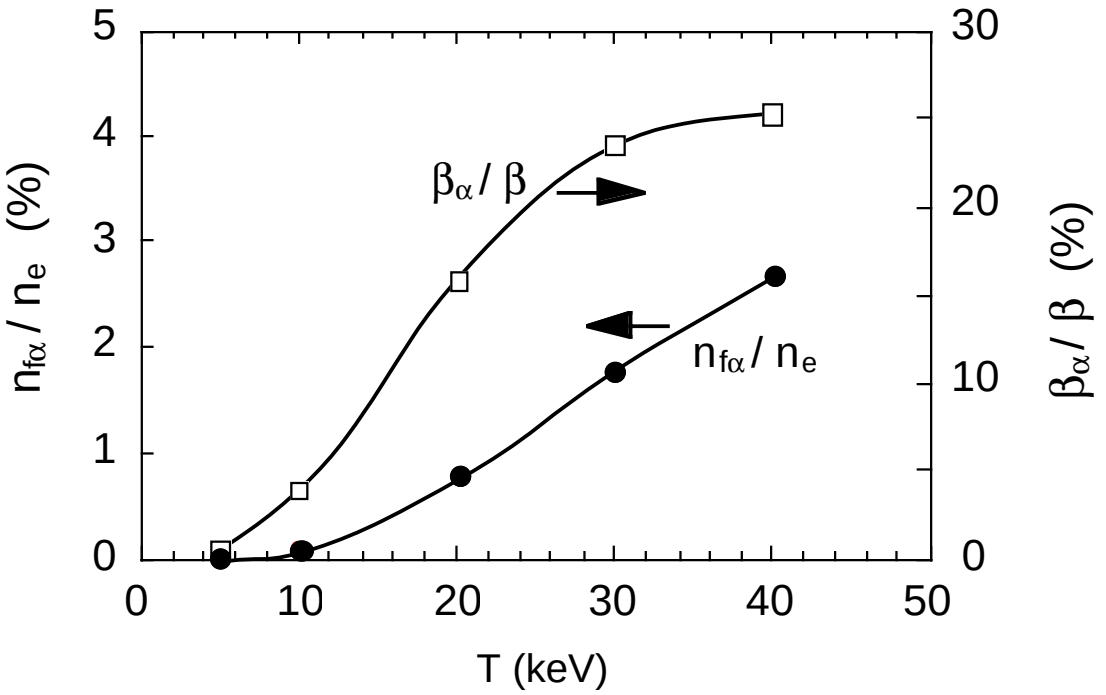

FIG. 5-1. Local values of n_α/n_e and β_α/β, for the case of $T_i \sim T_e \sim T$ and $Z_{eff} = 1.5$ (from Ref. [5.16]).

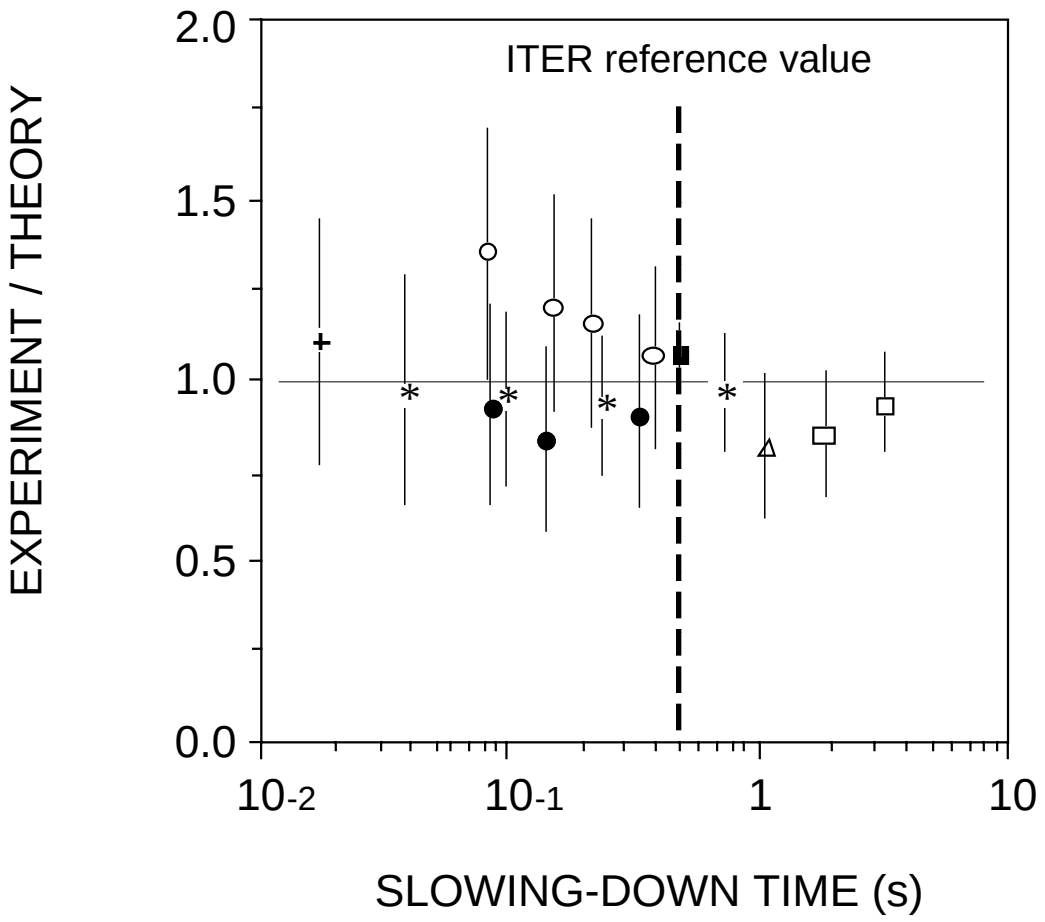

FIG. 5-2. Ratio of the measured slowing down time to that predicted by classical theory (modified from Fig. 20 in Ref. [5.3]). The data points denote 38-75 keV D-beam ions [▫] and DT alphas [■] in TFTR (from Ref. [5.12]), D-beam ions in DIII-D [○], 75 keV D-beam ions in DIII-D [●], 1 MeV triton fusion products in JET [▵], 250-400 keV D-beam ions in JT-60U [*] (from Ref. [5.13]), and 30 keV D-beam ions in ISX-B [+].

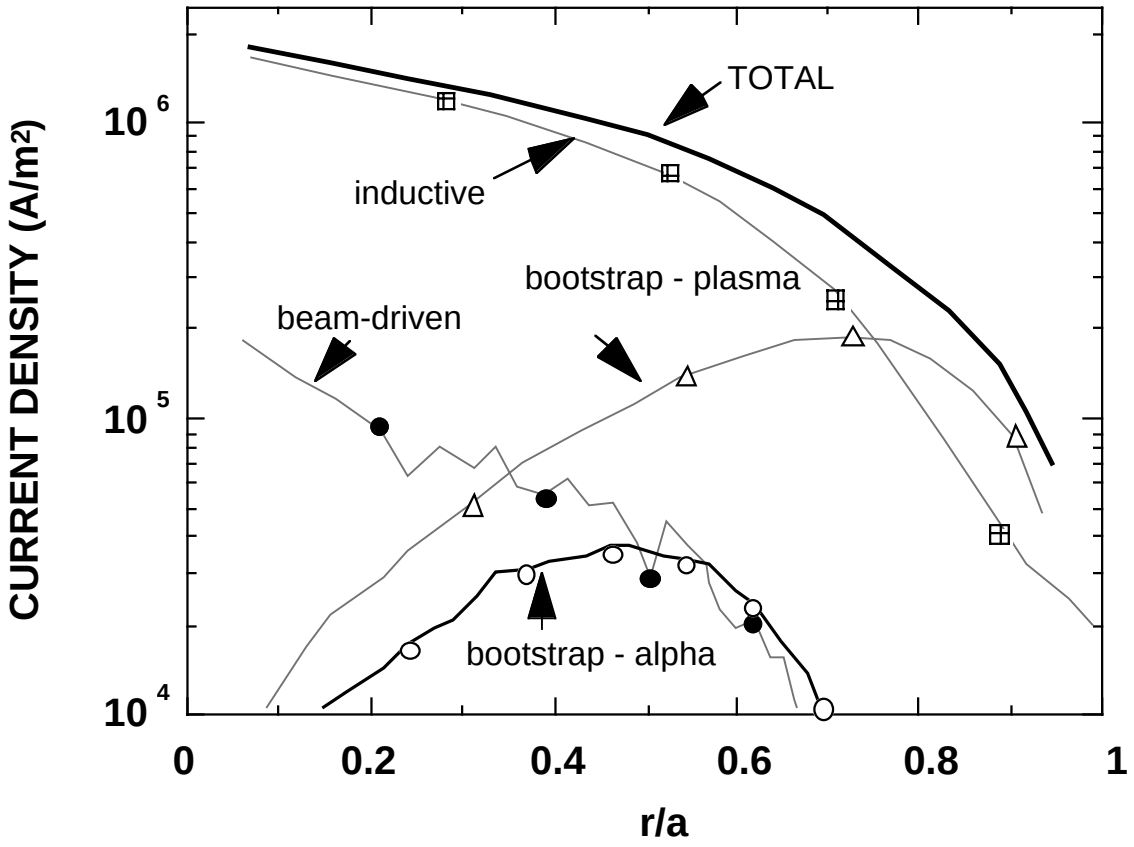

FIG. 5-3. Plasma current density profiles in a 21 MA ignited plasma with current drive provided by 1 MeV neutral beam injection. The plasma current consists of 15.27 MA of inductive current, 4.88 MA of bootstrap current (4.44 MA from the main plasma and 0.44 MA from the alpha particles), and 0.85 MA of beam-driven current.

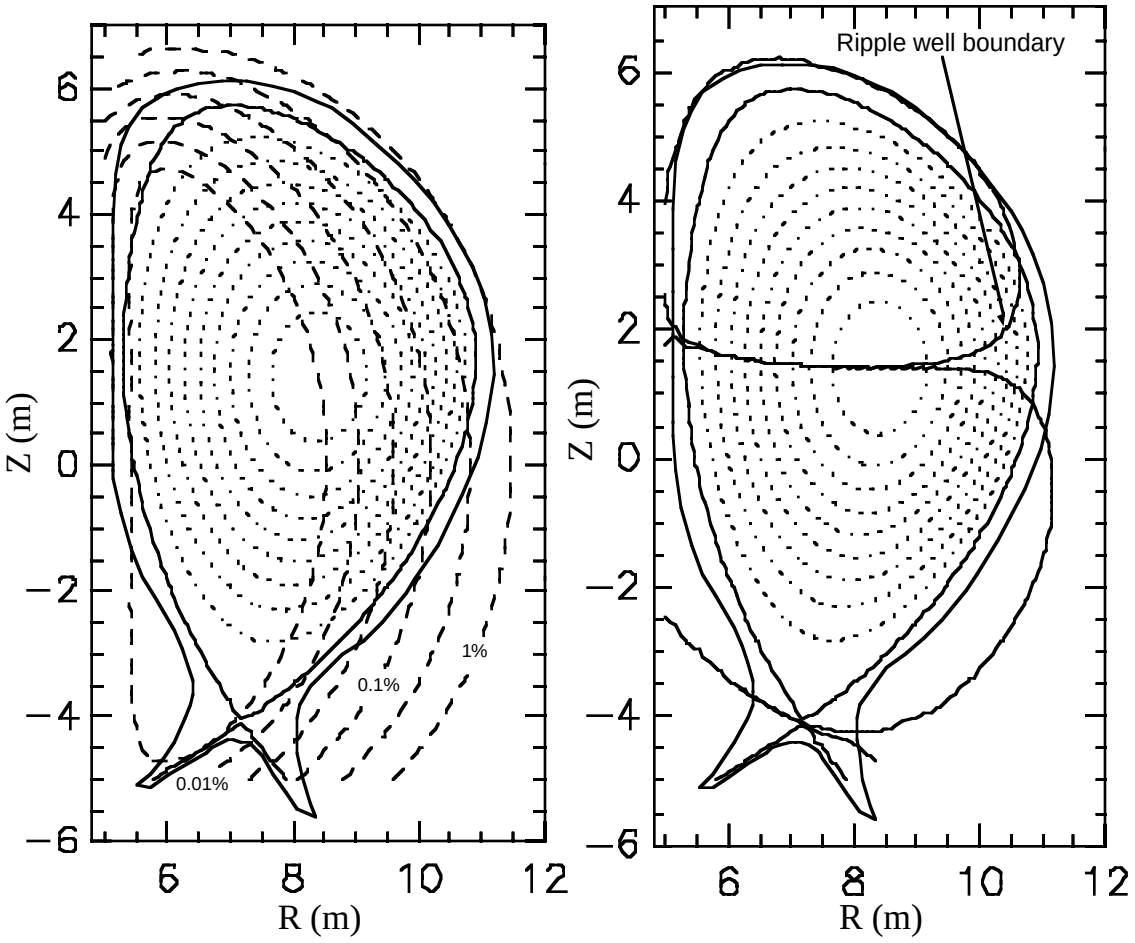

FIG. 5-4. TF ripple contours on the plasma cross section (left) and ripple well boundary (right), for the reference ITER plasma configuration with I_p = 21 MA.

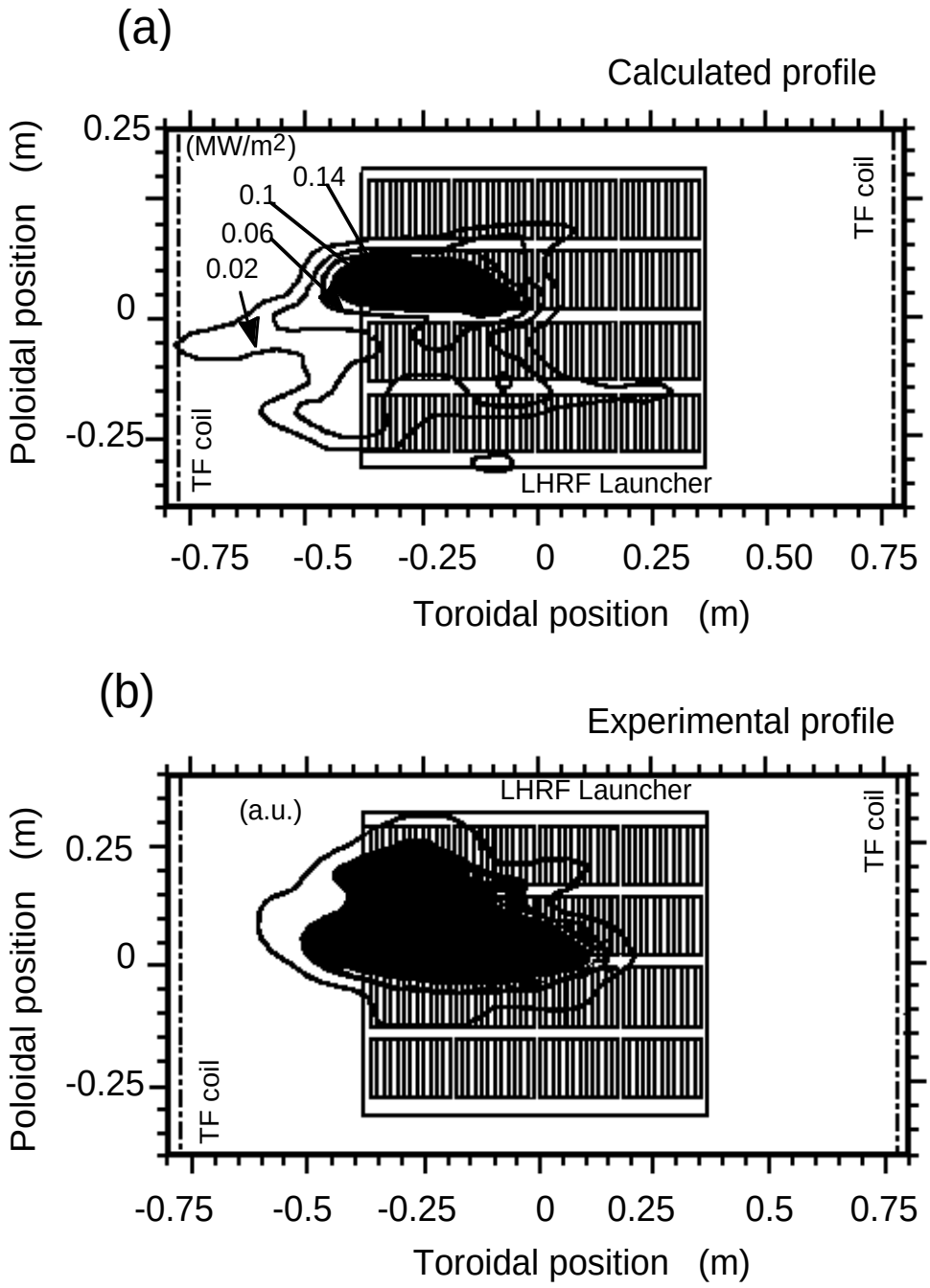

FIG. 5-5. Hot spots on the outboard first wall of JT-60U due to TF ripple loss of NBI ions, as calculated from the OFMC code and measured by an IRTV camera (from Ref. [5.31]): (a) the calculated 2-D heat deposition profile due to banana drift ripple loss; (b) the measured heating profile. The code successfully predicts the location and magnitude of this fast ion loss.

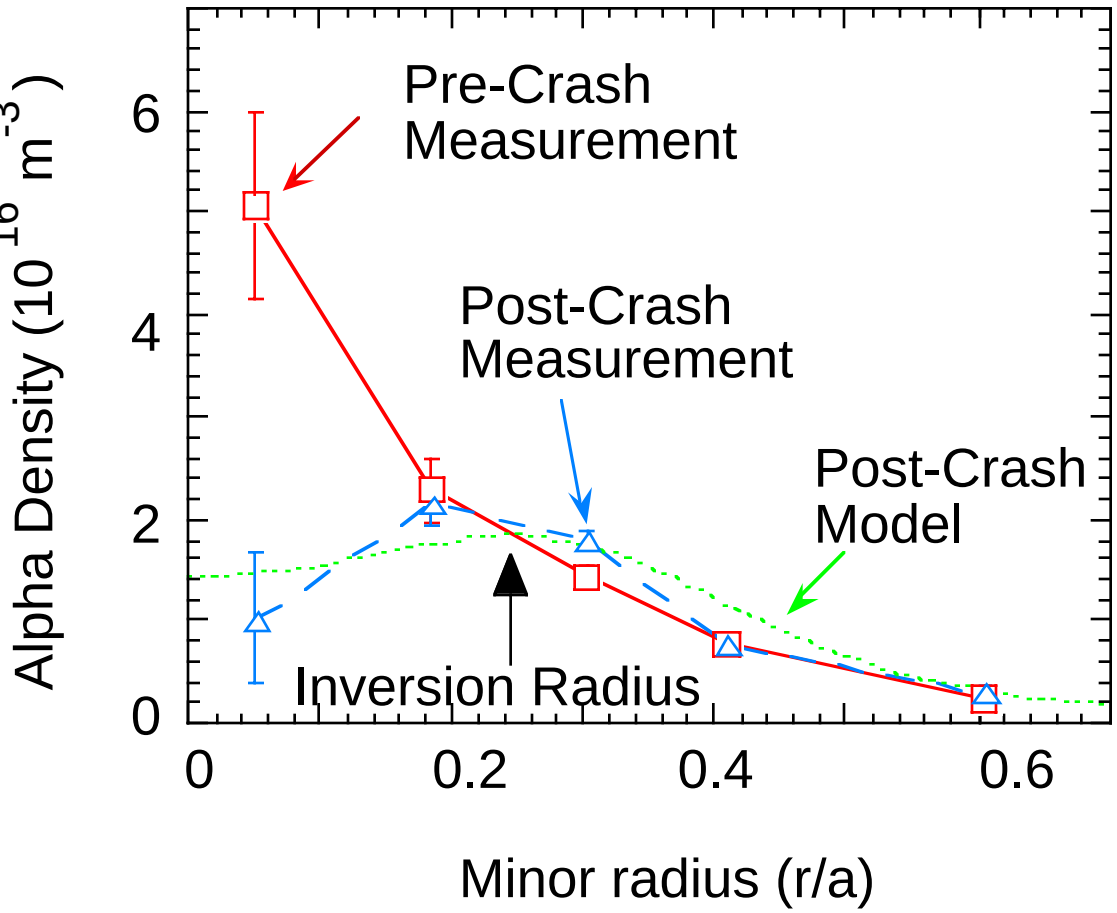

FIG. 5-6. Redistribution of partially thermalized alphas by a sawtooth crash in TFTR, as measured by the Alpha-CHERS diagnostic for confined alphas in the energy range 0.1-0.6 MeV (from Ref. [5.64]). The central alpha density drops by a factor of ≈5 after the sawtooth crash, while the alpha density outside the sawtooth inversion radius increases so that the total confined alpha density is constant. The central alpha density before the sawtooth crash is consistent with classical alpha confinement and thermalization.

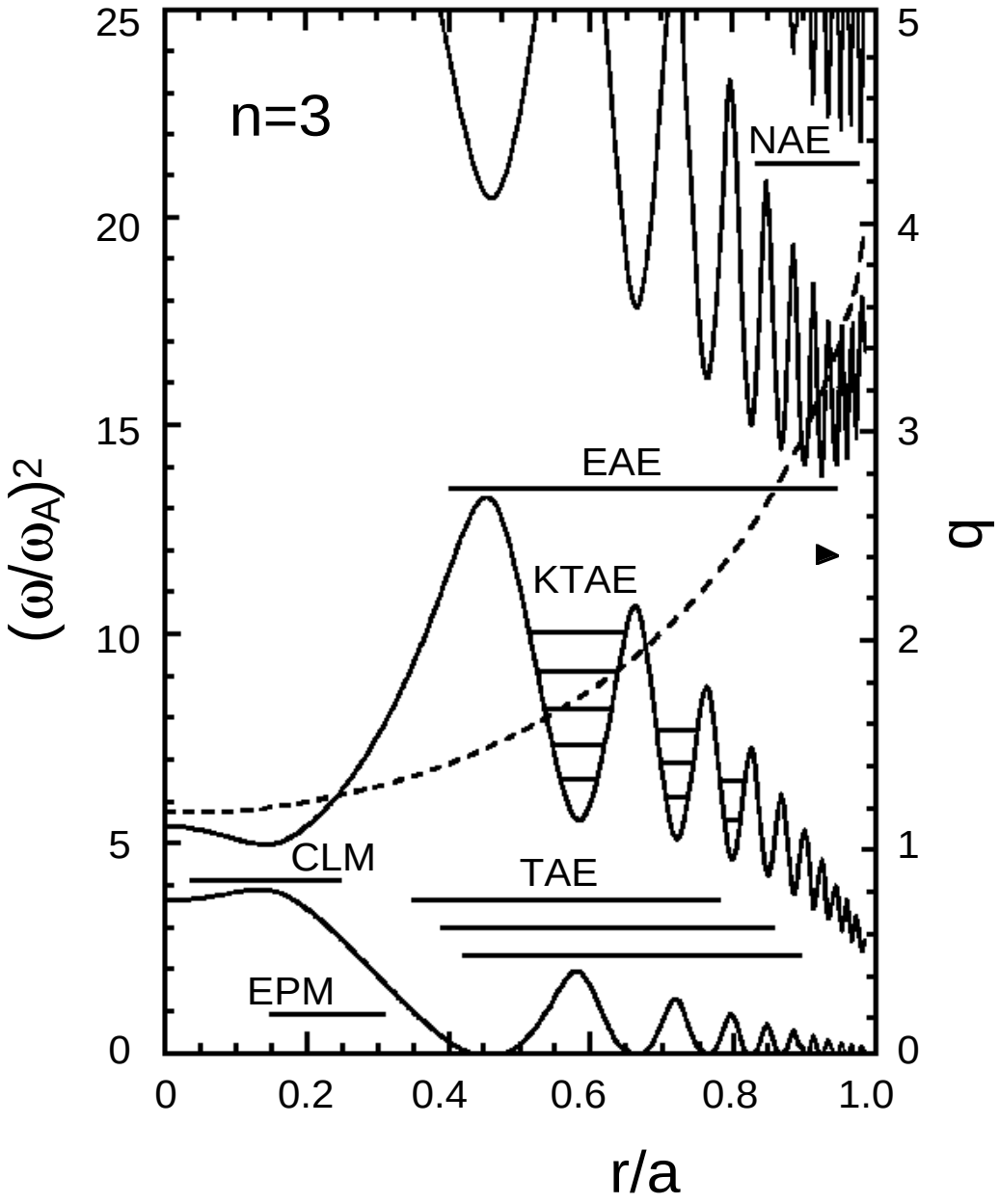

FIG. 5-7. Schematic showing representative shear Alfvén frequency continuum curves as functions of minor radius r, for n = 3, with horizontal lines indicating the approximate frequency, radial location, and mode width for the toroidicity Alfvén eigenmode (TAE), kinetic TAE mode (KTAE), core-localized TAE mode (CLM), ellipticity Alfvén eigenmode (EAE), triangularity Alfvén eigenmode (NAE), and energetic particle continuum mode (EPM). (Adapted from Ref. [5.118].)

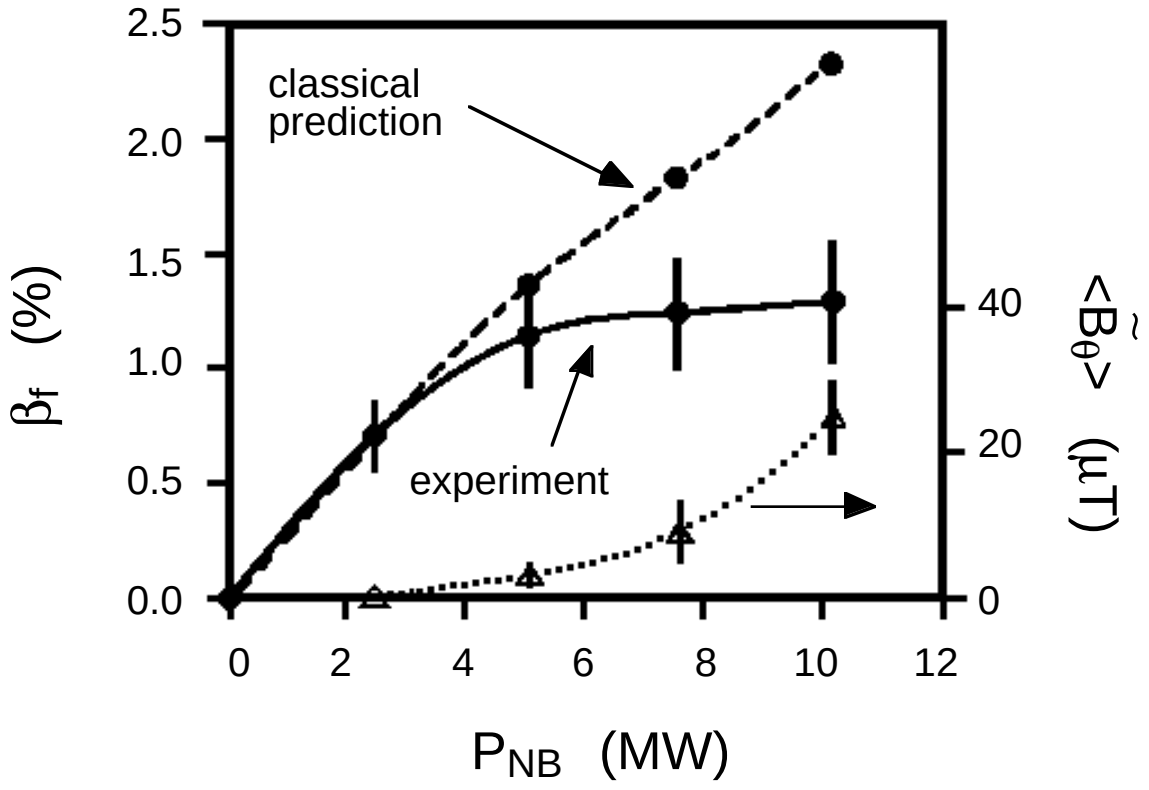

FIG. 5-8. TAE mode amplitude and fast ion beta during a scan of neutral beam heating power in DIII-D (from Ref. [5.108]). The TAE increases with the externally injected NBI power, but the fast ion beta does not increase as much as expected classically due to the TAE-induced NBI loss. At the highest TAE amplitudes, up to 70% of the NBI power can be lost due to TAE modes in DIII-D.

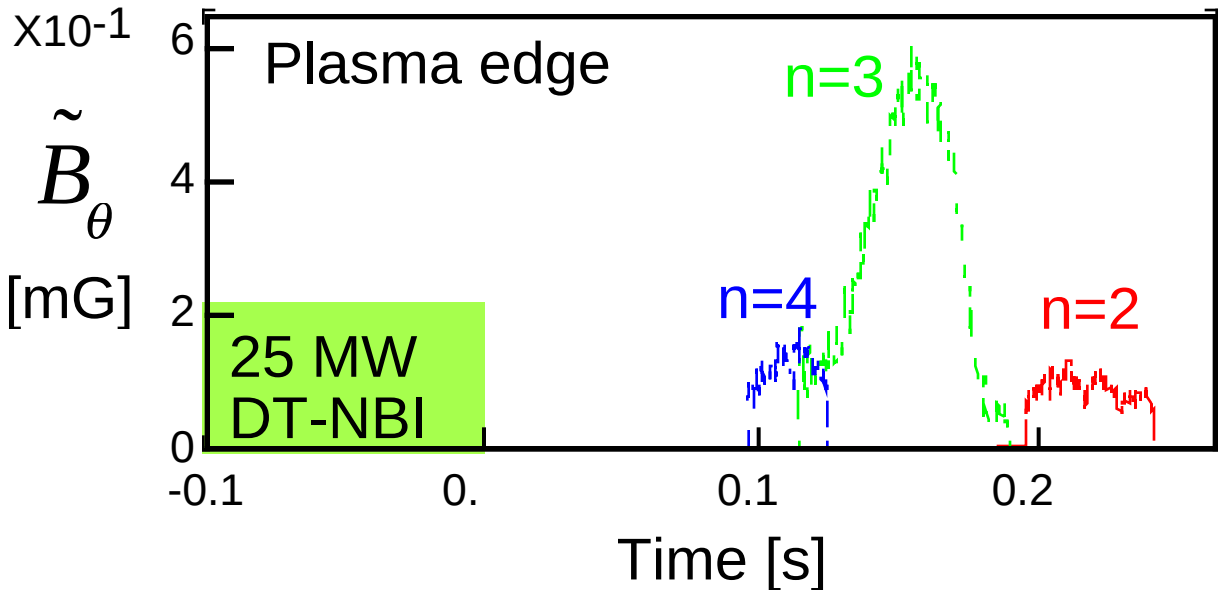

FIG. 5-9. Observation of alpha-driven TAE modes in TFTR (from Ref. [5.123]). The TAE modes appear ≈150 msec after the end of NBI in DT discharges with high q(0), consistent with theory in which the NBI ions damp the mode and the high q(0) increases the alpha particle drive. The amplitude of these external magnetic perturbations is several orders of magnitude smaller than the usual low frequency MHD modes in TFTR, so there was no perceptible alpha loss associated with these TAE modes.

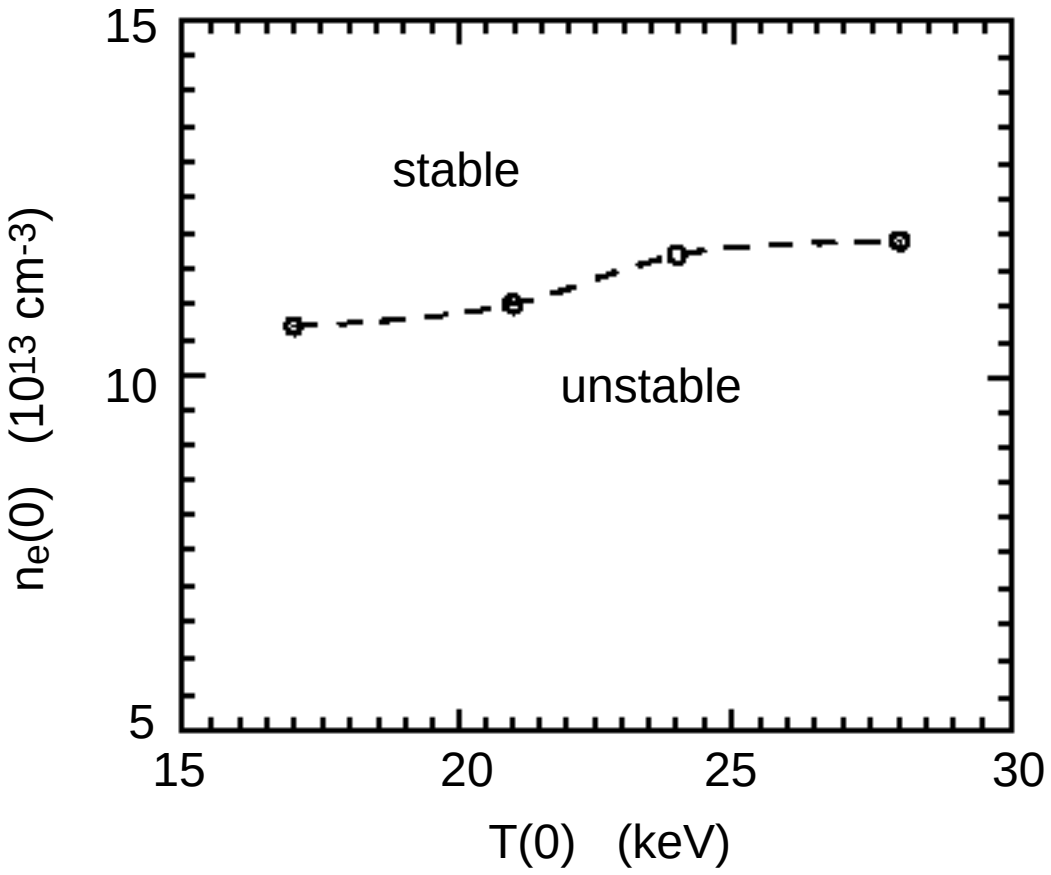

FIG. 5-10. Stability boundary in the ne(0)-T(0) POPCON diagram for an n = 15 core-localized TAE mode in an ITER-type plasma (from Ref. [5.158]).

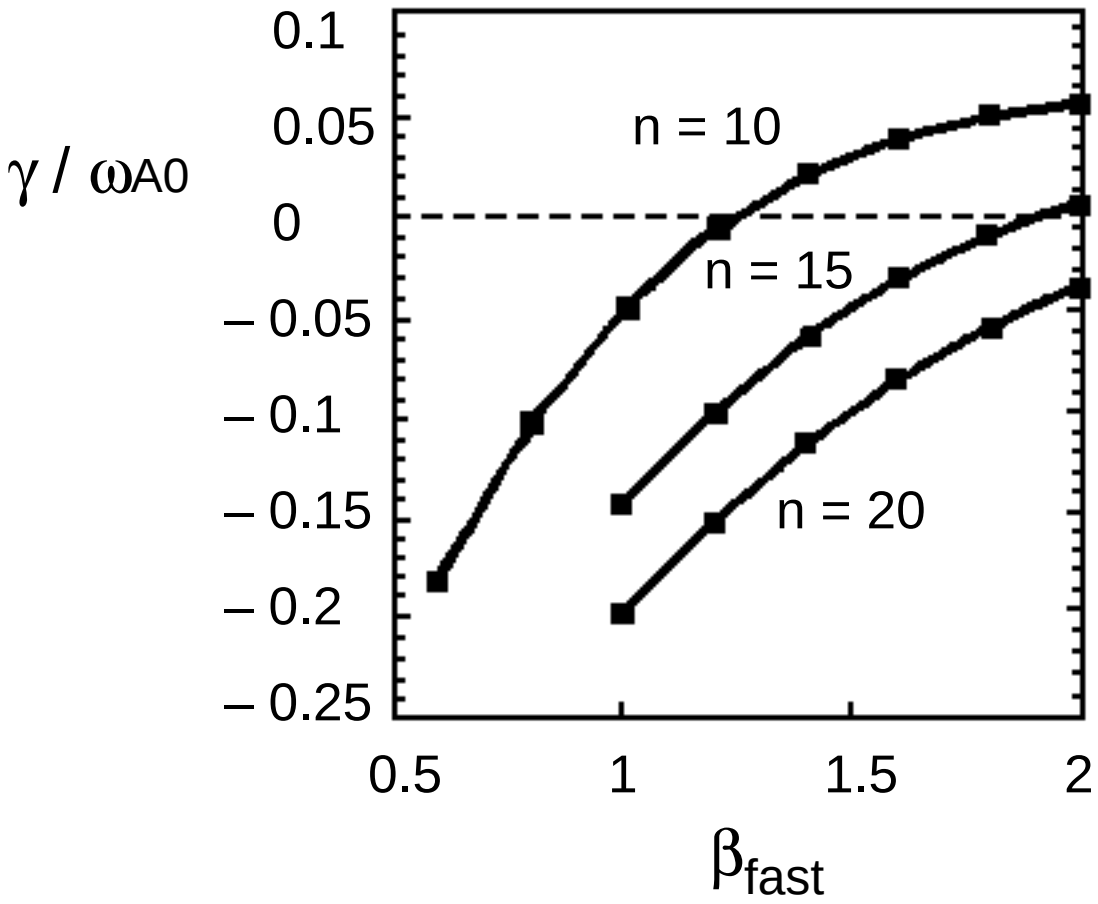

FIG. 5-11. Growth rate for the energetic particle-driven continuum mode as a function of the alpha particle beta value (normalized to the ITER reference value) for various toroidal mode numbers. (From Ref. [5.165])

[USE POSTSCRIPT FIGURE EMBEDDED IN CLARIS DRAW]

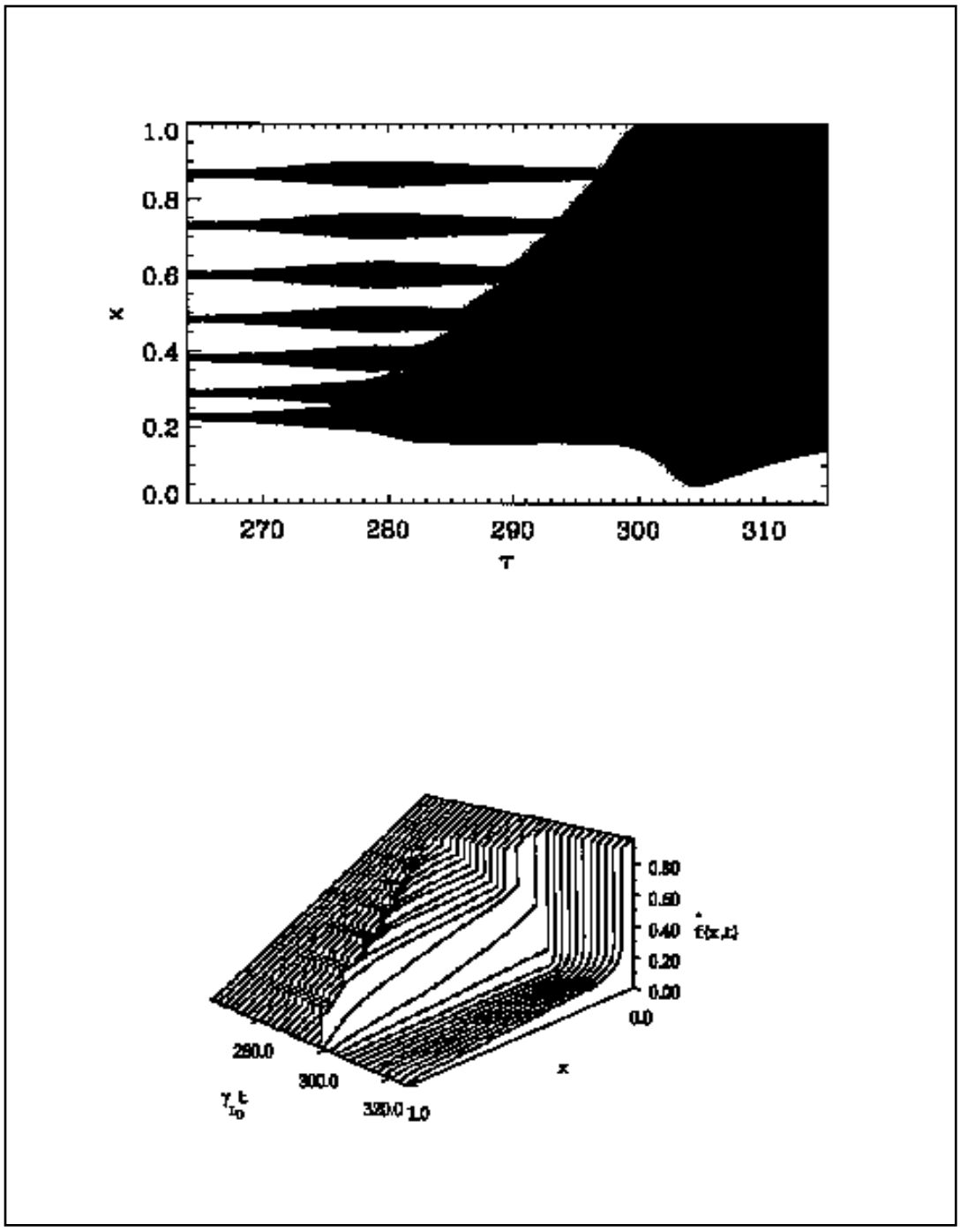

FIG. 5-12. Time evolution of (a) resonance widths for a multi-mode system and (b) resonant particle distribution function, where mode overlap leads to a “domino” avalanche and global diffusion of alpha particles. (From Ref. [5.184])

[USE POSTSCRIPT FIGURE EMBEDDED IN CLARIS DRAW]

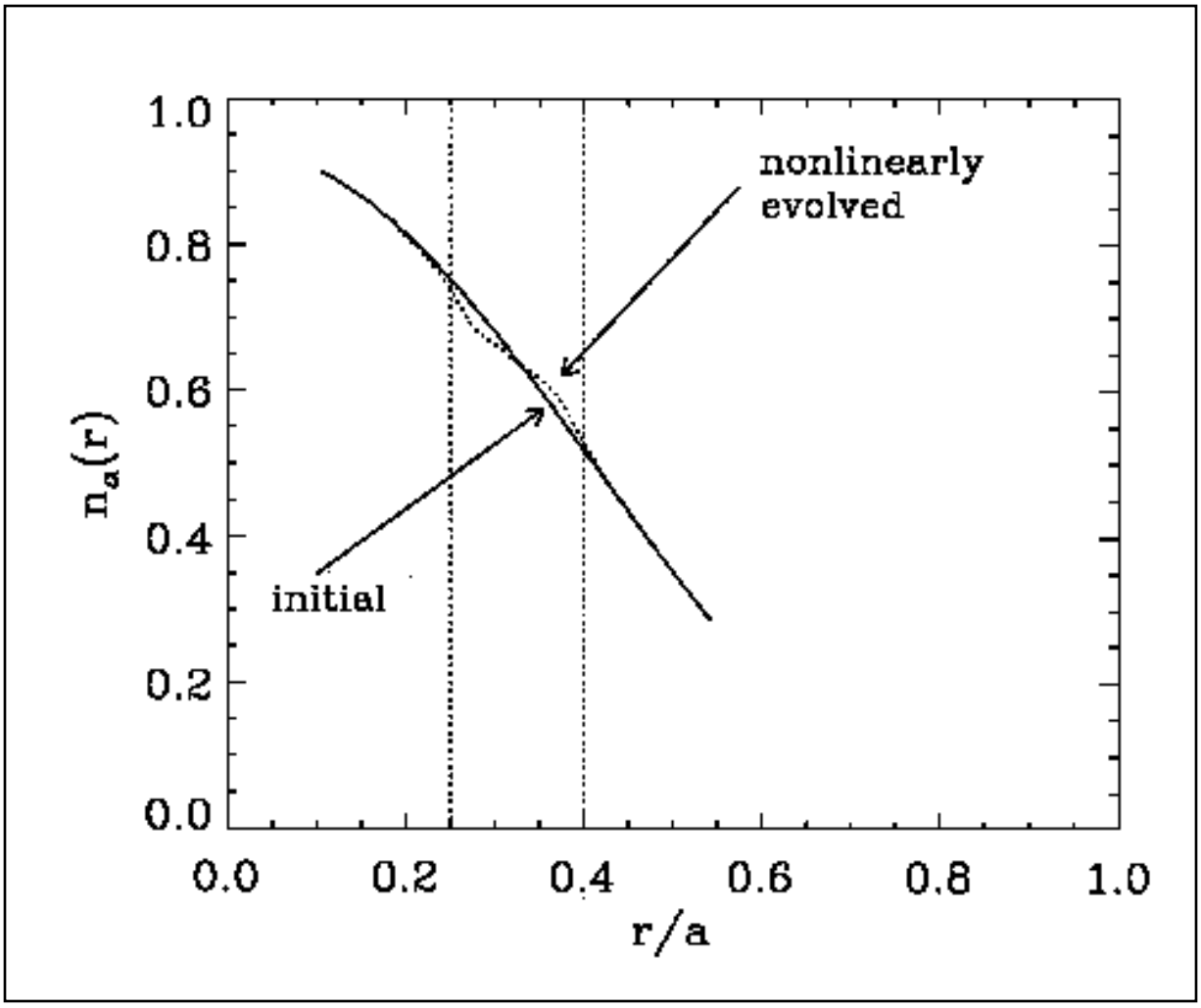

FIG. 5-13. Anomalous diffusion of the alpha particle distribution caused by 10 strongly unstable core-localized TAE modes in ITER. (From Ref. [5.185])